Measurement of R_c and n_c from charm counting in hadronic Z events

Th. Brenke[1], **M. Elsing**[2], **P.Sponholz**[1]
[1] Bergische Universität – Gesamthochschule Wuppertal, Germany
[2] CERN, Geneva, Switzerland

Abstract

Hadronic Z events collected with the DELPHI detector between 1994 and 1995 are used to measure the partial decay width R_c of the Z into $c\bar{c}$ quark pairs and the number of charm quarks n_c per b decay using the charm counting technique. Particle identification provided by the DELPHI Ring Imaging Cherenkov Counters and the Time Projection Chamber is used to obtain clear D^0, D^+, D_s^+, and Λ_c^+ signatures. The charm hadron production is measured in each channel from a simultaneous fit to the scaled energy, impact parameter information and the invariant mass spectra. The results obtained for R_c and n_c are

$$\begin{aligned} R_c &= 0.1757 \pm 0.0061(stat) \pm 0.0084(syst) \pm 0.0072(Br) \\ n_c &= 1.182 \pm 0.039(stat) \pm 0.068(syst) \pm 0.050(Br)\,, \end{aligned}$$

respectively.

1 Introduction

A precise determination of the partial decay width R_c of the Z into $c\bar{c}$ quark pairs provides a fundamental test of the standard model. The measurement of the number of charm quarks n_c per b decay is an important input to resolve the discrepancy between the experimental value of $BR(b \to l\nu X)$ and its theoretical prediction [1].

In this paper a simultaneous measurement of these quantities via the charm counting technique [2] is presented. The measured rate of D or Λ hadrons in $b\bar{b}$ and $c\bar{c}$ events is given by twice the product of the partial width $R_{c(b)}$ times the probability $P_{c(b)\to D,\Lambda}$ of the quark to produce a given charm hadron. For $c\bar{c}$ events the sum over the probabilities $P_{c\to D,\Lambda}$ for all weakly decaying charm hadrons adds up to one. Hence one can extract R_c from the sum of the rates. In $b\bar{b}$ events the sum of the production probabilities is a direct measurement of the number of charm quarks n_c per b decay. The large statistic available from the LEP I run yields to significant improvements in the precision compared to previous DELPHI results [3].

Since charm hadrons are produced both in $c\bar{c}$ and $b\bar{b}$ events, the separation between these flavors is necessary. A fit of the Monte Carlo b and c contributions to the measured impact parameter information, scaled energy $X_E = 2E_D/\sqrt{s}$ and invariant mass spectra is used to separate the classes. In this analysis charm hadrons are reconstructed in the following decay modes [1]:

- $D^0 \to K^-\pi^+$
- $D^+ \to K^-\pi^+\pi^+$
- $D_s^+ \to \phi(1020)\pi^+$
- $D_s^+ \to \bar{K}^*(892)K^+$
- $\Lambda_c^+ \to pK^-\pi^+$

Combinatorial background is largely reduced by identifying kaons and protons in the charm hadron decay products using particle identification information provided by the DELPHI Ring Imaging Cherenkov Counters (RICH) and the measured specific energy loss in the Time Projection Chamber (TPC).

2 The DELPHI detector

The DELPHI detector consists of several independent devices for tracking, calorimetry, lepton and particle identification. Only the tracking and particle identification components are relevant for this analysis and will be briefly described in the following. A detailed description of the whole apparatus and its performance can be found in [4].

Looking from the interaction point through the detector, the closest tracking device is the Vertex Detector (VD). The LEP I version of the detector was build up from three concentric layers of silicon micro strip modules with the outer layer having 11 cm radius. Since 1994 the single sided closer and outer layer have been replaced by double sided modules. With an intrinsic $R\phi$ resolution of 7.6 μm [4] the VD is the main component to

[1] Throughout this paper charge-conjugate states are implicitly included.

reconstruct secondary vertices of heavy hadron decays. The VD is followed by the Inner Detector (ID) which consists of a jet chamber part and a proportional chamber. The Time Projection Chamber is the main tracking device in DELPHI. Charged particles are measured with a precision of approximately 250 μm in $R\phi$ and 880 μm in z [4]. From the measured amplitudes on up to 192 sense wires the specific energy loss of charge particles (dE/dx) can be measured. The outermost tracking component for the barrel region is the Outer Detector (OD) made out of 5 layers of drift tubes. The DELPHI Barrel RICH is placed between the TPC and the Outer Detector. With its two radiators it is able to identify pions, kaons and protons over nearly the full momentum range. The use of particle identification information is described in section 4.

The charged tracking is extended to the forward region by two wire chambers FCA and FCB. FCA is mounted on the endcap of the TPC and covers a polar angle range from 11° to 32°, while FCB is placed behind the forward RICH on both sides of the DELPHI endcaps. FCB covers the polar angle range from 11° to 36°.

3 Event selection and Monte Carlo modelling

The starting point for the track selection is the primary vertex. It is determined for each event from the measured tracks with a constraint on the measured mean beam spot position. The fit is iterated until either the χ^2/NDF of all contributing tracks is ≤ 3 or at least 2 tracks are left. All track parameters are then redefined after a helix extrapolation to this vertex position. The resolution of tracks measured only by the forward tracking chambers is improved by a track refit using the primary vertex. Tracks having a fit $\chi^2 > 100$ are removed from the analysis. All tracks which satisfy the following conditions are retained for the analysis:

- track length $L_{track} > 30\ cm$
- momentum $p > 0.4\ GeV/c\ \ and\ \ p < 50\ GeV/c$
- relative error on momentum $\Delta p/p < 100\%$
- polar angle $20° \leq \theta \leq 160°$
- impact parameter to primary vertex $\epsilon_{R\phi} < 4.0\ cm\ \ and\ \ \epsilon_z < 10.0\ cm$

Events are then chosen, if the total charged energy is larger than 12% of the centre of mass energy and at least 5 charged particles are present. The numbers of hadronic events selected by this procedure are listed in table 1 for the different datasets. All events at centre of mass energies within 2 GeV to the Z resonance are used for the analysis. The efficiency for selecting hadronic Z events has been studied on the Monte Carlo and varies between 95.64% and 95.84% for the two years. The data sample contains 0.19% of bhabha and 0.24% of τ events. The bias in the number of events is taken into account in the following. All other backgrounds are found to be negligible.

The simulation is done with JETSET 7.4 Parton Shower [5] using DELPHI tuned parameters obtained from a fit to event shape distributions and identified particle spectra [6]. The heavy hadron decay tables were modified to include D^{**} and B^{**} production

Year	Data	Monte Carlo	selection efficiency
1994	1386191	3551362	95.64 %
1995	675100	1862256	95.84 %

Table 1: *Number of selected hadronic events for the different years of data taking. The efficiency is given in the last column.*

with rates of 30% B^{**} in $b\bar{b}$ events and 30% D^{**} in $c\bar{c}$ events. The fragmentation function used for b and c quarks is that of Peterson et al. [7]:

$$f(z) \propto \left[z \left(1 - \frac{1}{z} - \frac{\epsilon_q}{1-z} \right)^2 \right]^{-1} \tag{1}$$

In this function z denotes the fraction $(E+p_{||})_{hadron}/(E+p_{||})_{quark}$ with $p_{||}$ the momentum component parallel to the quark direction. The $\epsilon_{q=b,c}$ parameters are adjusted in order to reproduce the average energy fractions $\langle X_E^b(B) \rangle = 0.702 \pm 0.008$ and $\langle X_E^c(D^*) \rangle = 0.510 \pm 0.005 \pm 0.008$ taken by B and D^* hadrons in Z events [8], respectively.

4 Charm hadron reconstruction

The selection of charm hadrons is performed in two stages. In the first stage a set of loose kinematic cuts as given in table 2 and 3 are applied to reduce combinatorial background. The candidates then enter in a secondary vertex fit. In the second stage all quantities are calculated with the new track parameters belonging to the common vertex and the final cuts are applied.

Particle	$mass\,[GeV/c^2]$	X_E^{cut}
D^0	1.35 - 2.45	0.13
D^+	1.60 - 2.15	0.13
D_s^+	1.50 - 2.40	0.13
Λ_c^+	2.00 - 2.60	0.20

Table 2: *Preselection cut values on the invariant mass and the scaled energy.*

In a first step candidates for the charm hadron decays $D^0 \to K^-\pi^+$, $D^+ \to K^-\pi^+\pi^+$, $D_s^+ \to \phi(1020)\pi^+$, $D_s^+ \to \bar{K}^*(892)K^+$ and $\Lambda_c^+ \to pK^-\pi^+$ are reconstructed from all possible combinations of charged particles asking a minimal momentum above 1 (2) GeV/c for pion and kaon (proton) candidates. In addition a minimal momentum of 3 GeV/c is required for the ϕ and $\bar{K}^*$ from the decay of the D_s^+. Furthermore the invariant ϕ and $\bar{K}^*$ mass for these candidates is required to lay in between

$$\begin{aligned} 1.01\,GeV/c^2 &< m_\phi < 1.03\,GeV/c^2 \\ 0.86\,GeV/c^2 &< m_{\bar{K}^*} < 0.94\,GeV/c^2\,, \end{aligned}$$

respectively. Candidates for a given decay are retained if their scaled energy X_E and invariant mass satisfy the cuts given in table 2.

To reject the bulk of the combinatorial background a cut on the helicity angle is done. This quantity denotes the angle between the sphericity axis of the decay products in the rest frame of the charm hadron (D or Λ) with respect to its direction of flight. The pseudo scalar charm ground states decays are isotropic in this angle while the combinatorial background has a clear enhancement at $\cos\Theta_h = \pm 1$. Since the background is concentrated at lower energies than charm hadrons, energy dependent cuts in the helicity angle distribution

$$X_E > a \cdot e^{+b(\cos\Theta_h - 1)} - c \tag{2}$$

and

$$X_E > a \cdot e^{-b(\cos\Theta_h + 1)} - c \tag{3}$$

are used, which decrease in strength with increasing energy. The corresponding coefficients are listed in table 3.

Particle	a	b	c
D^0	0.5	4.0	0.15
D^+	0.5	3.0	0.05
D_s^+	0.5	2.2	0.10
Λ_c^+	0.5	3.0	0.10

Table 3: *Parameters for the energy dependent cut values on the helicity angle for the preselection of candidates.*

A full vertex fit is performed for all candidates accepted after the preselection cuts. The track parameters of all decay products are recalculated assuming the common vertex position. After the vertex reconstruction tighter cuts as given in tables 4 and 5 are applied for the final selection of the candidates.

Particle	$mass\,[GeV/c^2]$	X_E^{cut}
D^0	1.80 - 2.20	0.30
D^+	1.70 - 2.05	0.20
D_s^+	1.90 - 2.20	0.20
Λ_c^+	2.10 - 2.50	0.30

Table 4: *Final cut values on the invariant mass and the scaled energy.*

With the presence of secondary vertices the computation of the charm candidate's decay length ΔL and the vertex quality is possible for a further reduction of the combinatorial background. ΔL is calculated as the distance between the primary and the decay vertex in the xy plane, projected on the charm direction of flight. The sign of the decay

Particle	a	b	c
D^0	0.5	2.0	0.20
D^+	0.5	3.0	0.10
D_s^+	0.5	3.0	0.10
Λ_c^+	0.5	3.0	0.15

Table 5: *Energy dependent cut values on the helicity angle for the final selection.*

length is set negative if the decay vertex is behind the primary vertex w.r.t. the direction of flight. A positive value of ΔL is required in order to remove combinatorial background due to combinations of tracks from the primary vertex. To allow for the much lower combinatorial background level at large energies an additional energy dependent decay length cut is introduced:

$$\Delta L(X_E) > x \cdot (X_E - X_E^{cut})^2 + y \quad \text{and} \quad \Delta\mathrm{L} > \Delta\mathrm{L}_{\mathrm{cut}}\,. \tag{4}$$

The coefficients x and y together with the fixed cut in ΔL are listed in table 6 for the different decay channels. The value X_E^{cut} is the one given in table 4. No energy dependent cut is used for the Λ_c and the $D_s^+(\bar{K}^*)$ sample. Here the best signal to background ratio is found using harder cuts on ΔL.

Particle	x	y	ΔL_{cut} cm
D^0	-0.5	0.125	0.050
D^+	-1.0	0.230	0.125
$D_s^+(\phi)$	-1.0	0.100	0
$D_s^+(\bar{K}^*)$	-	-	0.100
Λ_c^+	-	-	0.015

Table 6: *Cuts on the decay length and parameters for the energy dependent decay length cut.*

For the $D_s^+(\phi)$ sample an additional cut is made on the angle $\Theta_{K\pi}$ between one of the kaons from the ϕ and the remaining pion in the rest frame of the ϕ. This angle follows a $cos^2(\Theta_{K\pi})$ distribution because of the spin structure of the decay, while the background is flat. A cut on $cos(\Theta_{K\pi}) > 0.3$ is used for the $D_s^+(\phi)$ sample, whereas the $D_s^+(\bar{K}^*)$ sample shows no significant improvement in using such a cut within errors.

Another kinematic quantity used to remove background is the probability $\mathcal{P}(\chi^2)$ of the secondary vertex χ^2. For well measured secondary vertices the probability is flat between 0 and 1, while it peaks at 0 for bad combinations. For the D^+, $D_s^+(\phi)$ and Λ_c^+ decay modes a cut of $\mathcal{P}(\chi^2) > 0.001$ is used, while a tighter cut of 0.01 is applied for the $D_s^+(\bar{K}^*)$ channel. No cut is applied on the two body decay vertex of the D^0. All tracks associated to the charm hadron candidate are required to have at least one associated VD hit in order to remove badly measured tracks from secondary interactions.

The particle identification provided by the DELPHI RICH and the specific energy loss dE/dx measurement in the TPC is used to further remove combinatorial background. To

illustrate the performance of the particle identification, a $D^{*+} \to D^0\pi^+$ sample is used to obtain a high purity kaon and pion sample from the $D^0 \to K^-\pi^+$ decay . The response from the RICH gas and liquid radiators on this sample is shown in figure 1. The same sample is used in figure 2 to show the measured energy loss of kaons and pions at energies above 1.5 GeV.

The tagging of the kaons and protons from the charm hadron decay is done using DELPHI standard tagging routines for the RICH [9] and the dE/dx [4] identification. For the RICH the measured Cherenkov angle information is translated into π, K and p tagging words. In addition a heavy tag (HV) is constructed to separate pions from kaons and protons. The quality of the RICH information is summarised into different levels for the quality flag. See reference [9] for details. Table 7 summarises the tagging cuts done for the different decays.

The dE/dx information is tested only if no RICH information is available for a track. Here the tagging is done using the *pull* of the measured dE/dx w.r.t. the expected value for a given particle type. To separate kaons from pions or protons from kaons a cut parameter tag_{TPC} is calculated on the basis of a simple ansatz for the probability density P^{TPC}:

$$tag_{TPC} = \frac{P^{TPC}_{K/p}}{P^{TPC}_{K/p} + P^{TPC}_{\pi/K}} \tag{5}$$

$$P^{TPC}_{K/\pi/p} = e^{-\frac{1}{2}pull^2_{K/\pi/p}}. \tag{6}$$

Again the cut values are given in table 7. To ensure a good energy loss measurement quality flags similar to the RICH information are tested. For all decay modes except the D^0, a candidate kaon or proton track is rejected if no RICH or dE/dx identification is available.

Decay	tagged	RICH NEWTAG				dE/dx		reject
	particle	flag	π tag	HV tag	p tag	flag	tag	no id.?
$D^0 \to K^-\pi^+$	K^-	≥ 2	< 1	-	-	-	≥ 0.3	no
$D^+ \to K^-\pi^+\pi^+$	K^-	≥ 2	< 1	-	-	≥ 1	≥ 0.2	yes
$D_s^+ \to \phi(1020)\pi^+$	K^-	≥ 2	< 1	-	-	≥ 1	≥ 0.2	yes
$D_s^+ \to \bar{K}^*(892)K^+$	K^-	≥ 1	< 1	-	-	≥ 1	≥ 0.2	yes
	K^+	≥ 1	-	≥ 1	-	≥ 1	≥ 0.2	yes
$\Lambda_c^+ \to pK^-\pi^+$	K^-	≥ 1	-	≥ 1	-	-	-	yes
	p	≥ 2	-	-	≥ 0	-	-	yes

Table 7: *Cuts applied on kaon and proton candidates using the standard RICH and dE/dx tagging information. See text for details of the tagging words.*

The D^0, D^+, D_s^+ and Λ_c^+ obtained after this selection are shown in figures 4 to 7. The reflections from other D decay modes are shown as the dotted lines. D^+ decays into $K^-K^+\pi^+$ or $K^-\pi^+\pi^+$, where the wrong mass is assigned to one of the pions, is an important background in the D_s^+ spectra, as can be seen in figures 5 and 6. An additional cut is applied to D^+ sample to remove background from $D^{*+} \to D^0\pi^+$ decays, where

the D^0 decays into $K^-\pi^+$. The difference between the $K^-\pi^+\pi^+$ and any of the $K^-\pi^+$ combinations has to be above 150 MeV/c^2.

5 Fit method

For a measurement of R_c and n_c it is necessary to distinguish the charm production in $c\bar{c}$ and $b\bar{b}$ events in an optimal way in order to keep correlations small. To achieve the best separation, the scaled energy of the charm hadron is used together with the impact parameter tag [11] in a combined fit.

The impact parameter information of each charged particle track is used to define the probability $\mathcal{P}_{ev}$ that all tracks are compatible with a common primary vertex. For details of the calculation see reference [11]. Since the distribution peaks around zero for $b\bar{b}$ events, a transformation

$$tr(\mathcal{P}_{ev}) = \frac{4}{4 - ln(\mathcal{P}_{ev})} \tag{7}$$

is applied to stretch this area. The selection of charm hadrons results in a sample of events with tracks having large impact parameters, especially for the D^+ sample because of its long lifetime. Hence $\mathcal{P}_{ev}$ is computed only from all tracks in the event which are not used to reconstruct the charm hadron candidate.

The use of the X_E distribution reflects that charm hadrons from $c\bar{c}$ events have a harder energy spectrum than those coming from B decays. Combining both variables allows to separate the background form light quark events from $b\bar{b}$ and $c\bar{c}$ events. Light quark events are expected to have large $tr(\mathcal{P}_{ev})$ and small X_E, while both other classes are either concentrated at small $tr(\mathcal{P}_{ev})$ or large X_E.

The charm hadron X_E and $tr(\mathcal{P}_{ev})$ distributions for the different decay modes are shown in figures 8 to 17. The combinatorial background is subtracted from the data using a fit of the Monte Carlo background to the sidebands of the signals. No correction for the reconstruction efficiency is applied. The Monte Carlo rates of charm hadrons in $c\bar{c}$ and $b\bar{b}$ events are scaled with the final fit results.

Particle	$mass$	X_E	$tr(\mathcal{P}_{ev})$	$\langle N^{dat}_{i,j,k} \rangle$
D^0	10	5	5	139
D^+	10	6	6	126
$D_s^+(\phi)$	8	4	4	31
$D_s^+(\bar{K}^*)$	8	4	4	20
Λ_c^+	12	4	4	16

Table 8: *Number of bins used in each dimension and the average number of events per bin.*

The fit of the charm hadron rates $R_q \cdot P_{q\to X} \cdot BR$ in $c\bar{c}$ and $b\bar{b}$ events is binned in three dimensions X_E, $tr(\mathcal{P}_{ev})$ and invariant mass. The number of bins in each dimension and the average number of data events per bin are listed in table 8. The width of each bin is chosen to keep the number of events per bin about constant. The fit is done with two

different approaches depending on the average number of entries per bin. For the D^0 and D^+ this number is around 130 and this allows for each channel to perform a χ^2 fit:

$$\chi^2 = \sum_i^{mass} \sum_j^{tr(\mathcal{P}_{ev})} \sum_k^{X_E} \left(\frac{N^{dat}_{i,j,k} - \lambda_{i,j,k}}{\sigma_{i,j,k}} \right)^2 . \tag{8}$$

Here $N^{dat}_{i,j,k}$ is the number of data events in a given bin, $\sigma_{i,j,k}$ is the quadratic sum of the statistical error of the data and the Monte Carlo prediction. The expected number of events $\lambda_{i,j,k}$ is calculated assuming the Monte Carlo shape from the different classes. $\lambda_{i,j,k}$ is given by:

$$\begin{aligned} \lambda_{i,j,k} &= \frac{2N_{had}}{\epsilon_{had}} \sum_{q=b,c,g\to c\bar{c}} R_q \cdot P_{q\to X} \cdot BR \cdot \frac{\epsilon_{i,j,k} N^{signal}_{i,j,k}(q)}{N^{signal}_{tot}(q)} \\ &\quad + N^{back}_{i,j,k} \cdot n^{back}_{j,k} + N^{reflect}_{i,j,k} . \end{aligned} \tag{9}$$

The first term of this equation reflects the charm hadron signal with its contributions from $b\bar{b}$, $c\bar{c}$ and light quark events. The ratio $N^{signal}_{i,j,k}(q)$ over $N^{signal}_{tot}(q)$ denotes the flavour dependent shape of the signal in the Monte Carlo including the reconstruction efficiency $\epsilon_{i,j,k}$. The total number of hadronic events N_{had} and the selection efficiency ϵ_{had} is given in table 1.

The second term describes the Monte Carlo background shape. Here the $N^{back}_{i,j,k}$ rates include an overall normalisation obtained from a fit of the Monte Carlo invariant mass spectra to the data in the sidebands of the signal. The $n^{back}_{j,k}$ are additional background normalisations for each bin in X_E and $tr(\mathcal{P}_{ev})$. They are introduced to allow for little fluctuations in the Monte Carlo background description.

The rate of charm hadrons from $b\bar{b}$ and $c\bar{c}$ events $R_q \cdot P_{q\to X} \cdot BR$ as well as the background normalisation $n^{back}_{j,k}$ in each bin in X_E and $tr(\mathcal{P}_{ev})$ are free parameters in the fit. The rate of charm hadrons in light quark events is determined by the rate of gluon splitting into heavy quarks. The rate is fixed to the world average value [8].

Figure 18 shows the background normalisations as determined in the fit for the D^0 and D^+ where 5×5 and 6×6 separating bins in X_E and $tr(\mathcal{P}_{ev})$ have been chosen, respectively. The mean values are 0.994 and 0.978, the RMS is 0.092 and 0.100, respectively. Since the overall normalisation of the combinatorial background should be preserved, an additional term was added to the overall χ^2:

$$\chi^2 = \left(\frac{R-1}{\sigma_R} \right)^2 \tag{10}$$

with

$$R = \frac{\sum_i^{mass} \sum_j^{tr(\mathcal{P}_{ev})} \sum_k^{X_E} N^{back}_{i,j,k} \cdot n^{back}_{j,k}}{\sum_i^{mass} \sum_j^{tr(\mathcal{P}_{ev})} \sum_k^{X_E} N^{back}_{i,j,k}} . \tag{11}$$

The last contribution to the expectation is a term accounting for reflections from other decay modes, which are in particular necessary for the channel $D_s^+(\bar{K}^*)$ (see figure 6). They have been taken directly from the Monte Carlo.

For the D_s^+ and Λ_c the average number of entries is only around 20. Therefore the number of entries per bin is no longer Gaussian distributed and a Poissonian statistic is taken instead. The fit is done maximising the Likelihood:

$$\mathcal{L} = \sum_{i}^{mass} \sum_{j}^{tr(\mathcal{P}_{ev})} \sum_{k}^{X_E} \ln \left(\frac{\lambda_{i,j,k}^{N_{i,j,k}^{dat}}}{e^{\lambda_{i,j,k}} \cdot N_{i,j,k}^{dat}!} \right) . \tag{12}$$

Again, the equivalent R term is added to the likelihood.

6 Systematic uncertainties

Three major systematic error sources are considered for this analysis. The uncertainty in the Monte Carlo modelling of heavy quark production and decay can lead to changes in the predicted spectra of charm hadrons in $c\bar{c}$ and $b\bar{b}$ events. Problems in the simulation of the detector response on charm hadron events can affect the efficiency estimates. The fit method itself is also a potential source of systematic errors. The breakdown of the relative systematic errors on the measurements of $R_c P_{c\to D,\Lambda} BR$ and $R_b P_{b\to D,\Lambda} BR$ are given in tables 9 and 10, respectively.

Source	D^0	D^+	$D_s^+(\phi)$	$D_s^+(\bar{K}^*)$	Λ_c^+
$\tau(B^+, B^0, B_s^0, \Lambda_c)$ (see text)	$\mp$ 0.7	$\mp$ 0.6	$\mp$ 0.8	$\mp$ 1.1	$\mp$ 0.6
$\langle X_E^c(D^*)\rangle = 0.510 \pm 0.009$	$\pm$ 3.5	$\pm$ 2.4	$\pm$ 2.3	$\pm$ 2.8	$\pm$ 2.2
$\langle X_E^b(B)\rangle = 0.702 \pm 0.008$	$\pm$ 0.2	$\pm$ 0.3	$\pm$ 0.3	$\pm$ 0.4	$\pm$ 0.1
$\epsilon_{b\to D} = 0.42 \pm 0.07$	$\mp$ 0.6	$\mp$ 0.6	$\mp$ 0.7	$\mp$ 0.5	$\mp$ 0.2
$f(D^+, D_s^+, \Lambda_c)$ (see text)	$\mp$ 0.3	$\mp$ 0.6	$\mp$ 1.0	$\mp$ 0.5	$\mp$ 0.2
$\tau(D^+, D^0, D_s^+, \Lambda_c)$ (see text)	$\pm$ 0.7	$\pm$ 0.8	$\pm$ 1.1	$\pm$ 2.7	$\pm$ 1.6
$n_{g\to c\bar{c}} = (2.38 \pm 0.48)\%$	$\mp$ 0.4	$\mp$ 0.3	$\mp$ 0.3	$\mp$ 0.4	$\mp$ 0.2
Rich(+dE/dx)	$\pm$ 0.7	$\pm$ 2.4	$\pm$ 2.4	$\pm$ 3.6	$\pm$ 2.3
$\Delta L\, vs.\, X_E$	$\pm$ 3.1	$\pm$ 2.7	$\pm$ 1.8	$\pm$ 2.9	$\pm$ 2.4
$\mathcal{P}(\chi^2)$	-	$\pm$ 1.8	$\pm$ 1.8	$\pm$ 2.0	$\pm$ 1.8
VD-hits	$\pm$ 1.0	$\pm$ 1.3	$\pm$ 1.3	$\pm$ 1.3	$\pm$ 1.3
Tracking	$\pm$ 2.0	$\pm$ 3.0	$\pm$ 3.0	$\pm$ 3.0	$\pm$ 3.0
MC-Statistics	$\pm$ 2.2	$\pm$ 2.5	$\pm$ 9.3	$\pm$ 12.4	$\pm$ 10.7
$m(D, \Lambda)$ mean	$\pm$ 0.3	$\pm$ 0.2	$\pm$ 3.7	$\pm$ 4.4	$\pm$ 1.4
$m(D, \Lambda)$ width	$\pm$ 0.2	$\pm$ 0.2	$\pm$ 1.3	$\pm$ 2.6	$\pm$ 0.6
Reflections	$\mp$ 0.1	$\mp$ 0.7	$\mp$ 0.4	$\mp$ 4.9	$\mp$ 0.6
Binning	$\pm$ 0.5	$\pm$ 3.0	$\pm$ 4.0	$\pm$ 4.0	$\pm$ 2.0
Total	$\pm$ 5.8	$\pm$ 7.1	$\pm$12.15	$\pm$16.5	$\pm$ 13.3

Table 9: *Relative systematic error on* $R_c P_{c\to D,\Lambda} BR$ *in %.*

The Monte Carlo modelling of heavy flavour production and decay affects the fit result in different ways. A change of the parameters leads to a different shape of the Monte Carlo signal spectra. Furthermore the selection efficiency and lifetime tagging is depending on

Source	D^0	D^+	$D_s^+(\phi)$	$D_s^+(\bar{K}^*)$	Λ_c^+
$\tau(B^+, B^0, B_s^0, \Lambda_b)$ (see text)	$\pm$ 2.5	$\pm$ 2.4	$\pm$ 2.7	$\pm$ 2.9	$\pm$ 3.7
$\langle X_E^c(D^*)\rangle = 0.510 \pm 0.009$	$\mp$ 1.2	$\mp$ 1.1	$\mp$ 0.2	$\mp$ 0.5	$\mp$ 0.9
$\langle X_E^b(B)\rangle = 0.702 \pm 0.008$	$\pm$ 3.2	$\pm$ 1.9	$\pm$ 1.9	$\pm$ 2.8	$\pm$ 2.9
$\epsilon_{b\to D} = 0.42 \pm 0.07$	$\mp$ 3.9	$\mp$ 1.2	$\mp$ 1.3	$\mp$ 3.0	$\mp$ 1.0
$f(D^+, D_s^+, \Lambda_c)$ (see text)	$\pm$ 0.2	$\pm$ 0.1	$\pm$ 0.3	$\pm$ 0.3	$\pm$ 0.2
$\tau(D^+, D^0, D_s^+, \Lambda_c)$ (see text)	$\pm$ 0.3	$\pm$ 0.4	$\pm$ 0.2	$\pm$ 0.1	$\pm$ 0.2
$n_{g\to c\bar{c}} = (2.38 \pm 0.48)\%$	$\mp$ 0.3	$\mp$ 0.2	$\mp$ 0.2	$\mp$ 0.2	$\mp$ 0.3
Rich(+dE/dx)	$\pm$ 0.7	$\pm$ 2.4	$\pm$ 2.4	$\pm$ 3.6	$\pm$ 2.3
$\Delta L\, vs.\, X_E$	$\pm$ 3.1	$\pm$ 2.7	$\pm$ 1.8	$\pm$ 2.9	$\pm$ 2.4
$\mathcal{P}(\chi^2)$	-	$\pm$ 1.8	$\pm$ 1.8	$\pm$ 2.0	$\pm$ 1.8
VD-hits	$\pm$ 1.0	$\pm$ 1.3	$\pm$ 1.3	$\pm$ 1.3	$\pm$ 1.3
Tracking	$\pm$ 2.0	$\pm$ 3.0	$\pm$ 3.0	$\pm$ 3.0	$\pm$ 3.0
MC-Statistics	$\pm$ 2.7	$\pm$ 3.4	$\pm$ 6.1	$\pm$ 5.8	$\pm$ 4.5
$m(D, \Lambda)$ mean	$\pm$ 0.3	$\pm$ 0.3	$\pm$ 1.5	$\pm$ 3.4	$\pm$ 0.4
$m(D, \Lambda)$ width	$\pm$ 0.2	$\pm$ 0.1	$\pm$ 0.6	$\pm$ 4.4	$\pm$ 0.9
Reflections	$\mp$ 0.1	$\mp$ 0.5	$\mp$ 0.2	$\mp$ 1.9	$\mp$ 0.8
Binning	$\pm$ 0.6	$\pm$ 2.5	$\pm$ 2.0	$\pm$ 2.0	$\pm$ 3.0
Total	$\pm$ 7.4	$\pm$ 7.6	$\pm$ 8.9	$\pm$11.5	$\pm$10.3

Table 10: *Relative systematic error on* $R_b P_{b\to D,\Lambda} BR$ *in %.*

the heavy flavour production and decay properties. Therefore it is necessary to correct for inadequate simulation settings. The corrections are done using JETSET to produce the required distribution and compare it to the one given in the full simulation before detector acceptance. The ratio of the two spectra is used as a weight to modify the Monte Carlo shape in equation 9. To estimate the systematic error the input value is changed within its error and the procedure is repeated.

The b lifetimes are corrected separately for B^+, B^0, Λ_b and B_s^0. Here the world averages $\tau(B^0) = 1.56 \pm 0.04$, $\tau(B^+) = 1.65 \pm 0.04$, $\tau(B_s^0) = 1.54 \pm 0.07$ and $\tau(\Lambda_b) = 1.22 \pm 0.05$ [12] are used to correct the simulation. For the systematic uncertainties belonging to this source all the b lifetime distributions are regenerated at the edges of their errors and the fit is performed again. Similar to this procedure the c lifetimes are also corrected separately for D^+, D^0, Λ_c and D_s^+. Here the values $\tau(D^0) = 0.415 \pm 0.004$, $\tau(D^+) = 1.057 \pm 0.015$, $\tau(D_s^+) = 0.467 \pm 0.017$ and $\tau(\Lambda_c) = 0.206 \pm 0.012$ from [8] are taken.

The separation between $b\bar{b}$ and $c\bar{c}$ events obtained from the impact parameter tag depends on the rate of D^+ and D^0 mesons in $c\bar{c}$ events. Therefore the rates of charm hadrons in the hemisphere opposite to the reconstructed D or Λ are fixed to the present averages $f(D^+) = 0.221 \pm 0.020$, $f(D_s^+) = 0.112 \pm 0.027$ and $f(c_{baryon}) = 0.084 \pm 0.022$ [21]. The D^0 rate is calculated form these numbers according to

$$f(D^0) = 1 - f(D^+) - f(D_s^+) - f(c_{baryon})\,. \tag{13}$$

A one sigma error variation on each fraction is included in the systematic error, leaving the D^0 fraction free to keep the sum constant.

To allow for the uncertainty of the mean $\langle X_E^c(D)\rangle$ and $\langle X_E^b(B)\rangle$ the procedure is quite similar. JETSET is used to generate the $\langle X_E\rangle$ distributions of all charm ground states according to $\langle X_E^c(D^*)\rangle = 0.510 \pm 0.005 \pm 0.008$, $\langle X_E^b(B)\rangle = 0.702 \pm 0.008$ [8]. The energy spectrum of D mesons in the B rest frame was measured by CLEO [13]. This $\langle X_E^b(D)\rangle$ spectrum includes the contributions from $B \to D\,X$ and $B \to D\bar{D}\,X$. It can be parameterised in terms of a Peterson function with $\epsilon_{b\to D} = 0.42 \pm 0.07$ [10].

The corrections are applied on all simulated charm ground state hadrons separately for $b\bar{b}$ and $c\bar{c}$ events. The resulting X_E distribution of the sum of all charm hadron ground states in $c\bar{c}$ events is found to be in agreement with the corresponding average of $\langle X_E^c(D^0, D^+)\rangle = 0.484 \pm 0.008$ [8]. Here the effect of gluon splitting is taken into account. The systematic uncertainties are calculated separately for $\langle X_E^c(D)\rangle$, $\langle X_E^b(B)\rangle$ and $\epsilon_{b\to D}$.

To account for gluon splitting into $c\bar{c}$ quark pairs, the $g \to c\bar{c}$ component is subtracted from the measured charm hadron spectra as a third component in the fit. Here the Monte Carlo prediction is scaled to reproduce the average value $n_{g\to c\bar{c}} = (2.38 \pm 0.48)\%$ [14]. The systematic uncertainty is obtained by varying the rate within the error.

A good description of the detector acceptance is needed to extract the efficiency correction from the Monte Carlo. Therefore a careful tuning to correct for residual problems in the Monte Carlo description is done in all stages of the analysis. The decay channel $D^{*+} \to (K^-\pi^+)\pi^+$ is chosen to study the systematic errors due to the selection of charm hadrons. The D^{*+} sample is analysed in a window around the mass difference between the D^0 and the remaining slow π^+. For a cut applied to reconstruct a given decay channel, the inefficiencies $\bar{\epsilon}$ are computed in data from a fit to the corresponding D^{*+} mass spectrum of rejected events and compared to the Monte Carlo result. For a residual discrepancy between these inefficiencies a factor f_{corr}

$$f_{corr} = \frac{1 - \bar{\epsilon}_{data}}{1 - \bar{\epsilon}_{MC}} \tag{14}$$

is introduced to correct the Monte Carlo description of the efficiency. The relative statistical uncertainty of the correction factor is taken as the systematic error.

The combined RICH and dE/dx tagging used to reconstruct the different charm hadrons is tested using the kaon from the D^0 in the D^{*+} channel. For each decay mode the same cuts as given in table 7 are applied to the D^{*+} sample. To reconstruct the $D_s^+(\bar{K}^*)$ channel both kaons are required to be tagged. Here the correction applied is the product of two correction factors, one for the π veto on the K^- from $\bar{K}^*$ and one for the heavy tag on the K^+. A very tight $\Lambda^0 \to p\pi^-$ sample is used to test the proton identification for the Λ_c^+ channel. Only protons from Λ^0 with a momentum above the cut applied to the Λ_c^+ sample are used for this study.

The cut on the vertex fit χ^2 probability $\mathcal{P}(\chi^2)$ is also tested using the D^* sample. Fitting all three products of the $D^{*+} \to (K^-\pi^+)\pi^+$ decay into one common vertex is a good approximation for a three body decay vertex, since the pion from the D^{*+} decay has a small p_t w.r.t. the D^0.

The energy dependent cuts on the measured decay length ΔL of the charm hadron can be tested using the D^0 from the D^{*+} sample. The correction for the D^+ channel is computed scaling the measured D^0 decay length by the lifetime ratio of $\tau(D^+)/\tau(D^0)$.

The requirement of all candidate tracks to have at least one VD hit associated is again tested with the D^* decay, leaving out the slow pion in case of the D^0. A summary of all correction factors applied to the fitted rates can be found in table 11.

It has been checked that the product of the efficiency correction factors obtained is in good agreement with the overall correction for the VD hit, $\mathcal{P}(\chi^2)$, $Rich(+dE/dx)$ and $\Delta L\, vs.\, X_E$ cuts.

The charged track reconstruction efficiency is another possible source of systematic errors. In reference [15] the tracking efficiency in DELPHI has been determined to be 0.989 ± 0.001. The difference between data and Monte Carlo in the region of the TPC ϕ boundaries was estimated to be 0.2%. Following reference [15] the 1% inefficiency of the track reconstruction is used as the systematic error of the track reconstruction.

Particle	Rich(+dE/dx)	$\Delta L\, vs.\, X_E$	$\mathcal{P}(\chi^2)$	VD-hits
D^0	0.9961±0.0071	1.0121±0.0309	-	1.0182±0.0095
D^+	0.9962±0.0242	1.0172±0.0268	0.9316±0.0182	1.0184±0.0127
$D_s^+(\phi)$	0.9962±0.0242	1.0146±0.0175	0.9316±0.0182	1.0184±0.0127
$D_s^+(\bar{K}^*)$	0.9982±0.0360	0.9934±0.0287	0.9319±0.0204	1.0184±0.0127
Λ_c^+	0.9339±0.0226	1.0074±0.0235	0.9316±0.0182	1.0184±0.0127

Table 11: *Correction factors applied due to cut inefficiency discrepancies*

The systematic error due to the statistical error of the Monte Carlo is given in tables 9 and 10. For the D^0 and D^+ this error is included directly in the χ^2 definition. For the binned likelihood fit to the D_s^+ and Λ_c^+ spectra the error due to the limited number of Monte Carlo events is evaluated using a statistical method. The distribution of 3000 fit results using random Monte Carlo sets reflects the total statistical error while the error obtained from the fits only includes the statistical error of the data set itself. Hence the quadratic difference of both errors is taken as the contribution of the Monte Carlo statistical error.

The shape of the mass signal is a possible source of systematic errors. Therefore the variation of the mean and the width of the mass signal shape is included in the systematic error table.

The rate of reflections affect the background shape under the signal. Especially for the $D_s^+(\bar{K}^*)$ channel changes in the rates of the reflections lead to variations in the fit result. The systematic error assigned corresponds to a 30% variation of the reflection rates.

Finally the effect of the binning in the three dimensional fit is studied by varying the number of bins in each dimension by $\pm$ 1 bin. All systematic errors for the different decay channels are summed up quadratically to obtain the total systematic errors given in tables 9 and 10.

7 Fit results

From a three dimensional fit of the charm hadron *mass* spectra, the scaled energy X_E and the impact parameter information $tr(\mathcal{P}_{ev})$ the products $R_c P_{c\to D,\Lambda}\, BR$ and $R_b P_{b\to D,\Lambda}\, BR$ are measured. The results using the DELPHI data taken in 1994 and 1995 are shown in table 12. The first error denotes the statistical uncertainty, the second error corresponds to the systematic error discussed above. The numbers include the efficiency corrections given in table 11. The D_s^+ rates are corrected for the branching ratio $\phi \to K^-K^+ =$

$(49.1 \pm 0.6)\%$ [16] and $\bar{K}^*(892) \to K^-\pi^+ = 2/3$. The correlation between the measured production rates for $c\bar{c}$ and $b\bar{b}$ events is given in the last column.

Mode	$R_c P_{c\to D,\Lambda}\, BR \times 10^3$	$R_b P_{b\to D,\Lambda}\, BR \times 10^3$	*corr* %
$D^0 \to K^-\pi^+$	$3.663 \pm 0.125 \pm 0.214$	$4.950 \pm 0.199 \pm 0.371$	-45
$D^+ \to K^-\pi^+\pi^+$	$3.474 \pm 0.142 \pm 0.247$	$4.397 \pm 0.240 \pm 0.333$	-36
$D_s^+ \to \phi(1020)\pi^+$	$0.790 \pm 0.094 \pm 0.096$	$1.200 \pm 0.122 \pm 0.107$	-28
$D_s^+ \to \bar{K}^*(892)K^+$	$0.630 \pm 0.132 \pm 0.104$	$1.265 \pm 0.189 \pm 0.146$	-29
$\Lambda_c^+ \to pK^-\pi^+$	$0.907 \pm 0.193 \pm 0.121$	$1.098 \pm 0.226 \pm 0.113$	-28

Table 12: *Results on $R_{c(b)}P_{c(b)\to D,\Lambda}BR$ from the combined fit to the 1995 and 1994 data. The first error is statistical, the second belongs to systematics.*

Based on these numbers, the product of $R_{c(b)}$ and the production probability $P_{c(b)\to D,\Lambda}$ can be calculated using the branching ratios given in table 13 from reference [16].

Mode	branching ratio
$D^0 \to K^-\pi^+$	0.0383 ± 0.0012
$D^+ \to K^-\pi^+\pi^+$	0.091 ± 0.006
$D_s^+ \to \phi(1020)\pi^+$	0.035 ± 0.009
$\frac{BR(D_s^+\to\bar{K}^*K^+)}{BR(D_s^+\to\phi\pi^+)}$	0.95 ± 0.10
$\Lambda_c^+ \to pK^-\pi^+$	0.044 ± 0.006

Table 13: *Branching ratios used for the charm fraction measurements.*

No precise measurement for the branching ratio $D_s^+ \to \bar{K}^*(892)K^+$ has been done so far. Therefore the ratio $BR(D_s^+ \to \bar{K}^*(892)K^+)/BR(D_s^+ \to \phi(1020)\pi^+)$ is used. The results for both decay modes are compared in table 14. The third error given in addition to the statistical and systematic error corresponds to the uncertainty of the branching ratios. The average given in the table is computed taking all correlations into account. The statistical correlation of the averages for $c\bar{c}$ and $b\bar{b}$ events is -27%.

Mode	$R_c P_{c\to D_s^+} \times 10^2$	$R_b P_{b\to D_s^+} \times 10^2$
$D_s^+ \to \phi(1020)\pi^+$	$2.258 \pm 0.268 \pm 0.276 \pm 0.580$	$3.430 \pm 0.350 \pm 0.306 \pm 0.882$
$D_s^+ \to \bar{K}^*(892)K^+$	$1.893 \pm 0.397 \pm 0.313 \pm 0.525$	$3.802 \pm 0.559 \pm 0.440 \pm 1.056$
average	$2.123 \pm 0.223 \pm 0.217 \pm 0.533$	$3.535 \pm 0.300 \pm 0.273 \pm 0.885$

Table 14: *Results on $R_{c(b)}P_{c(b)\to D_s^+}$ including correlations*

A summary of the measured rates of D^0, D^+, D_s^+ and Λ_c^+ from $c\bar{c}$ and $b\bar{b}$ events is given in table 15.

Mode	$R_c P_{c\to D,\Lambda} \times 10^2$	$R_b P_{b\to D,\Lambda} \times 10^2$
D^0	$9.565 \pm 0.326 \pm 0.559 \pm 0.299$	$12.925 \pm 0.520 \pm 0.969 \pm 0.405$
D^+	$3.818 \pm 0.156 \pm 0.271 \pm 0.252$	$4.831 \pm 0.264 \pm 0.366 \pm 0.318$
D_s^+	$2.123 \pm 0.223 \pm 0.217 \pm 0.533$	$3.535 \pm 0.300 \pm 0.273 \pm 0.885$
Λ_c^+	$2.061 \pm 0.439 \pm 0.275 \pm 0.280$	$2.496 \pm 0.514 \pm 0.256 \pm 0.340$

Table 15: *Contributions to charm counting in $c\bar{c}$ and $b\bar{b}$ events. The first error is statistical, the second belongs to systematics and the third is due to the error on the branching ratio.*

8 Measurement of R_c

R_c is given by the sum of all weakly decaying charm hadron rates. The results presented in table 15 do not include strange charm baryon production. Following the argumentation in reference [2] and [8] the rates of these baryons are estimated from the light quark sector. The ratio Ξ^-/Λ is measured to be $(6.2 \pm 0.7)\%$ and the Ω^-/Λ ratio is $(0.5 \pm 0.3)\%$ [16]. Assuming equal production of Ξ^- and Ξ^0 one expects about 13% of strange charm baryon production relative to the Λ_c rate. The error assigned to this rate is 5%. Therefore a contribution of 0.00268 ± 0.00103 for Ξ_c and Ω_c is added to the measured rates. Taking correlated systematic errors into account one obtains:

$$R_c = 0.1757 \pm 0.0061(stat) \pm 0.0084(syst) \pm 0.0072(Br)\,. \tag{15}$$

A full set of parameters as used by the LEP heavy flavour working group is given in table 16 together with the correlation matrix.

parameter	value	error	R_c	$f(D^+)$	$f(D_s^+)$	$f(c_{bary})$
R_c	0.1757	0.0126	1.00	-.28	0.32	0.28
$f(D^+)$	0.2173	0.0216	-.28	1.00	-.32	-.30
$f(D_s^+)$	0.1211	0.0314	0.32	-.32	1.00	-.23
$f(c_{bary})$	0.1173	0.0302	0.28	-.30	-.23	1.00

Table 16: *Full set of parameters as used by the LEP heavy flavour working group with correlation matrix.*

9 Charm counting in b decays

To extract from table 15 the number of charm quarks per b decay one has to sum up all weakly decaying charm states. This includes charmonia $c\bar{c}$ states which count twice and strange charm baryons.

The $b \to$ *charmonia* rates given in table 17 have been measured by DELPHI [17]. From these numbers one can estimate the total rate of charmonia production in b decays

Mode	$P_{b\to X_c} \times 10^2$
J/ψ	$1.12 \pm 0.12(stat) \pm 0.10(sys)$
ψ'	$0.48 \pm 0.22(stat) \pm 0.10(sys)$
χ_{c1}	$1.4 \pm 0.6(stat)^{+0.4}_{-0.2}(sys)$

Table 17: *DELPHI published charmonia rates from b decays.*

assuming a ratio of $\eta_c : J/\psi : \chi_{c1} : \psi' = 0.57 : 1. : 0.27 : 0.31$ [18] for the different states. J/ψ and χ_{c1} production due to radiative charmonia decays are estimated using $BR(\psi' \to \chi_{c1}\gamma) = (8.7\pm0.8)\%$, $BR(\psi' \to J/\psi X) = (57\pm4)\%$ and $BR(\chi_{c1} \to J/\psi\gamma) = (27.3\pm1.6)\%$ [16]. One obtains $f(b \to charmonia\, X) = 0.0199 \pm 0.0029 \pm 0.0060$ for the total rate. The first error reflects the error of the measurements and of the branching ratios, the second error corresponds to a 30% uncertainty assigned to the theoretical prediction of reference [18].

Mode	$P_{b\to X_c} \times 10^2$
D^0	$59.56 \pm 2.39 \pm 4.46 \pm 1.86$
D^+	$22.27 \pm 1.22 \pm 1.69 \pm 1.47$
D_s^+	$16.29 \pm 1.38 \pm 1.25 \pm 4.08$
Λ_c^+	$11.50 \pm 2.37 \pm 1.18 \pm 1.56$
$charmonia(*2)$	$3.98 \pm 0.58 \pm 1.20$
total measured	$113.60 \pm 3.29 \pm 6.54 \pm 4.81$

Table 18: *Contributions to charm counting in $b\bar{b}$ events. The first error is statistical, the second belongs to systematics and the third is due to the branching ratios.*

The rates $R_b P_{b\to D,\Lambda}$ given in table 15 are translated into $P_{b\to D,\Lambda}$ using the present average $R_b = 0.2170 \pm 0.0009$ [21]. The summary of measured contributions to the charm counting in $b\bar{b}$ events is shown in table 18.

The production rate of $f(b \to \Xi_c X)$ is not measured. To estimate its value we follow the argumentation from reference [19]. CLEO [20] has measured the rates of $f(\bar{B} \to \Xi_c^+) = 0.008 \pm 0.005$ and $f(\bar{B} \to \Xi_c^0) = 0.012 \pm 0.009$. The PDG values[16] for rates of b hadrons in Z events are $(37.8\pm2.2)\%$ for B^0 and B^+, $(11.2\pm1.9)\%$ for B_s^0 and $(13.2\pm4.1)\%$ for b-baryons. One obtains a rate of 0.017 ± 0.010 Ξ_c baryons from B mesons. Using JETSET one estimates $f(b_{baryon} \to \Xi_c X) = 0.22 \pm 0.11$, which adds 0.029 ± 0.017 to the total Ξ_c rate. Adding the Ξ_c baryon contribution 0.046 ± 0.021 to the measured rates from table 18 one gets:

$$n_c = 1.182 \pm 0.039(stat) \pm 0.068(syst) \pm 0.050(Br)\,. \tag{16}$$

10 Conclusions

The results on R_c and n_c presented in this note are based on the DELPHI data taken in 1994 and 1995. The charm hadron production is measured from the D^0, D^+, D_s^+ and Λ_c signals using a simultaneous fit to the scaled energy, impact parameter information and the invariant mass spectra. The result on R_c significantly improves the precision compared to previous DELPHI results using the charm counting technique [3]. Good agreement is found with other LEP results [21] and the prediction of the standard model.

A comparison of the result on n_c presented in this note (together with the DELPHI results on semileptonic b branching ratio $B_{SL} = (10.64 \pm 0.13 \pm 0.24^{-27}_{+43})\%$ [22]) with the theoretical expectation from reference [23] is shown in figure 19. The result on n_c also agrees well with the other DELPHI result $n_c = 1.147 \pm 0.041$[24] using an indirect method to extract the charmless and double charm contribution from the b tagging spectrum. The results on the individual production rates in $b\bar{b}$ events agree well with numbers reported by OPAL [2] and ALEPH [19]. Only the different assumptions on strange charm baryon production give rise to larger differences between the measurements and to the result reported by CLEO [20].

A further improvement on the results presented in this note is expected using the full LEP I dataset including the 1992 and 1993 data taken by DELPHI.

11 Acknowledgements

We wish to thank Daniel Bloch (IReS Strasbourg) for the discussions during the whole period of the analysis and his constructive editing of this paper. We also like to thank our colleagues Jean-Pierre Engel (IReS Strasbourg) and Lionel Chaussard (IPN Lyon).

References

[1] G.Altarelli and S.Petrarca, Phys. Lett. **B 261** (1991) 303
I.Bigi et al., Phys. Lett. **B 323** (1994) 408

[2] G.Alexander et al., OPAL Collaboration, Z. Phys. **C 72** (1996) 1

[3] D.Bloch et al., *Summary of R_c Measurements in DELPHI*, DELPHI 96-110 CONF 37, Geneva 1996

[4] P.Abreu et al., DELPHI Collaboration, Nucl. Inst. and Meth. **A 378** (1996) 57

[5] T.Sjöstrand, Comp. Phys. Comm. **39** (1986) 347 ;
T.Sjöstrand and M.Bengtsson, Comp. Phys. Comm. **43** (1987) 367

[6] P.Abreu et al., DELPHI Collaboration, Zeit. Phys. **C 71** (1996) 11

[7] C.Peterson, D.Schlatter, J.Schmitt and P.Zerwas, Phys. Rev. **D27** (1983) 105

[8] The LEP Electroweak Working Group, *Presentation of LEP Electroweak Heavy Flavour Results for the Summer 1996 Conferences*, LEPHF/96-01, DELPHI 96-67 PHYS 627, Geneva 1996

[9] E.Schyns, *NEWTAG - π, K, p Tagging for Delphi RICHes*, DELPHI 96-103 RICH 89, Geneva 1996

[10] The LEP Electroweak Working Group, *A consistent treatment of systematic Errors for LEP electroweak Heavy Flavour Analyses*, LEPHF/94-01, DELPHI 94-23 PHYS 357

[11] G.V.Borisov, *Lifetime tag of events $Z^0 \to b\bar{b}$ with the DELPHI detector*, DELPHI 94-125 PROG 208, Geneva 1994

[12] L. Di Ciaccio, private communication, to be published in the PDG 98

[13] D.Bortoletto et al., CLEO Collaboration, Phys. Rev. **D 45** (1992) 21

[14] R. Akers et al., OPAL Collaboration, Phys. Lett. **B 353** (1995) 595

[15] P.Abreu et al., DELPHI Collaboration, *Measurement of the charged particle multiplicity of weakly decaying B hadrons*, CERN-PPE/98-34, Geneva 1998

[16] R.M.Barnett et al., Review of Particle Physics, Phys. Rev **D 54** (1996) 1

[17] P.Abreu et al., DELPHI Collaboration, Phys. Lett. **B 341** (1994) 109

[18] J.H.Kühn, S.Nussinov, R.Rüdel, Z. Phys. **C 5** (1980) 117

[19] D.Buskulic et al., ALEPH Collaboration, Phys. Lett. **B 388** (1996) 648

[20] L.Gibbons et al., CLEO Collaboration, Phys. Rev. **D 56** (1997) 3783

[21] The LEP Electroweak Working Group, *A Combination of Preliminary Electroweak Measurements and Constraints on the Standard Model*, CERN-PPE/97-154, Geneva 1997

[22] M.Calvi, P.Ronchese, *Measurement of the semileptonic b branching ratios and $\bar{\chi}_b$ from inclusive leptons in Z decays*, DELPHI 97-118 CONF 100, Geneva 1997

[23] M.Neubert and C.T.Sachrajda, Nucl. Phys. **B 483** (1997) 339

[24] P.Abreu et al., DELPHI Collaboration, *Measurement of the inclusive charmless and double-charm B branching ratios*, CERN-PPE/98-07, Geneva 1998

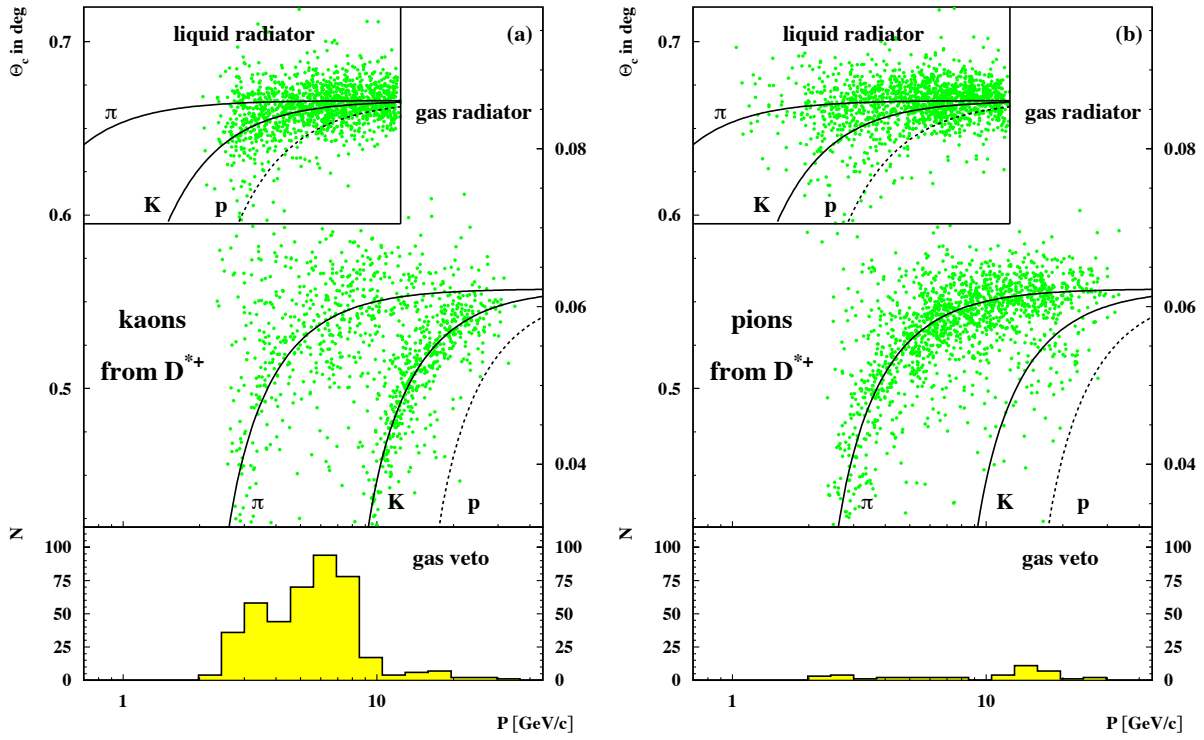

Figure 1: *The response of the DELPHI RICH gas and liquid radiators for (left) kaons and (right) pions from D^{*+} decay candidates. Shown is the measured Cherenkov angle in the gas radiator and the liquid radiator (insert), as well as the veto counts (lower part) as a function of the track momentum. The bands indicate the predicted Cherenkov angle for pions, kaons and proton.*

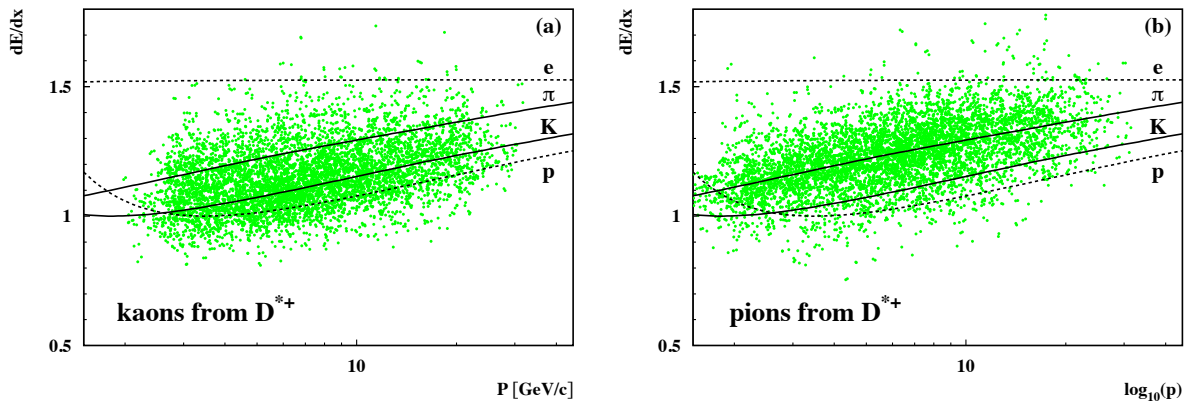

Figure 2: *The measured specific energy loss of (left) kaons and (right) pions from D^{*+} as a function of the track momentum. The expectation for kaons and pions is shown as lines.*

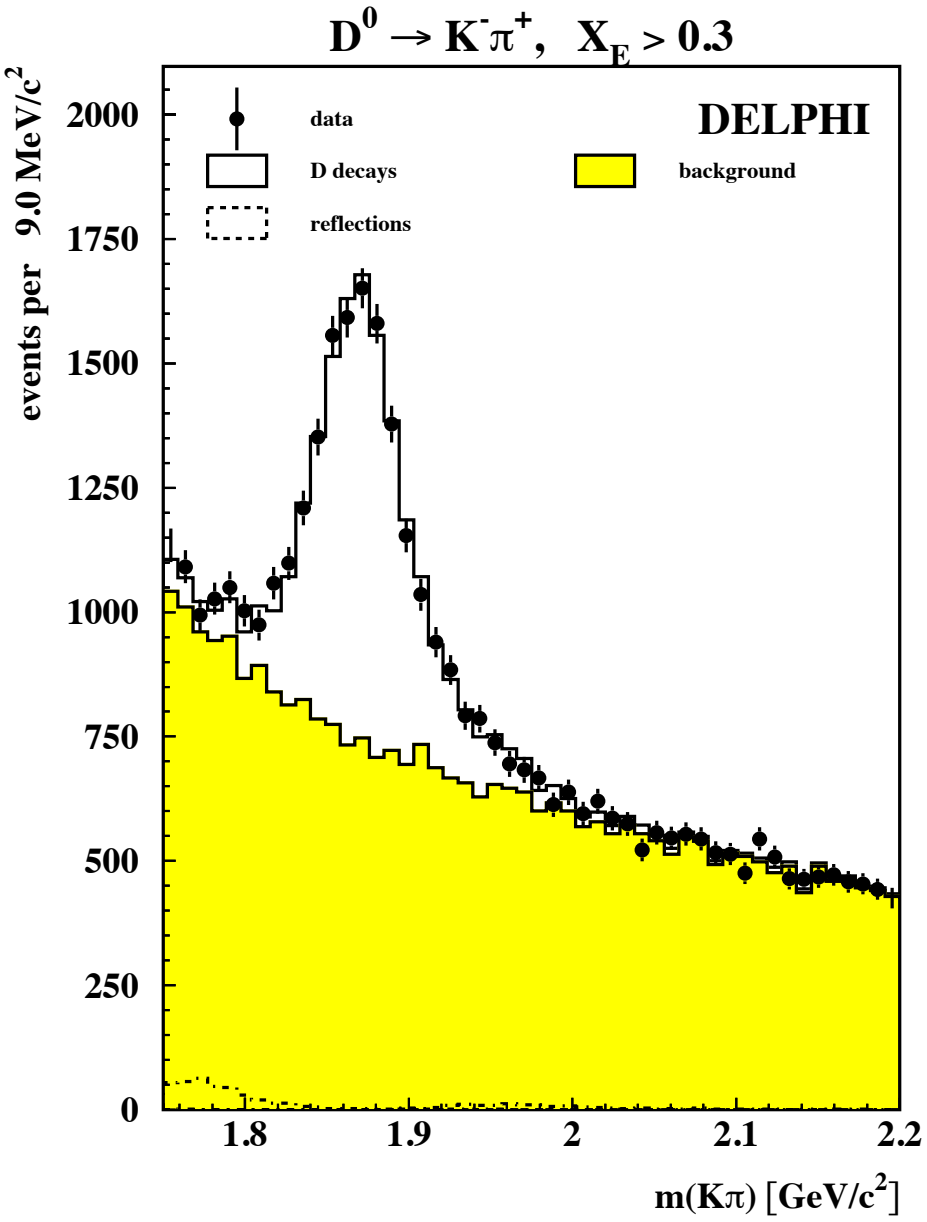

Figure 3: *Invariant $K\pi$ mass spectra showing the D^0 mass signal. Contributions from reflections are shown as a dotted line.*

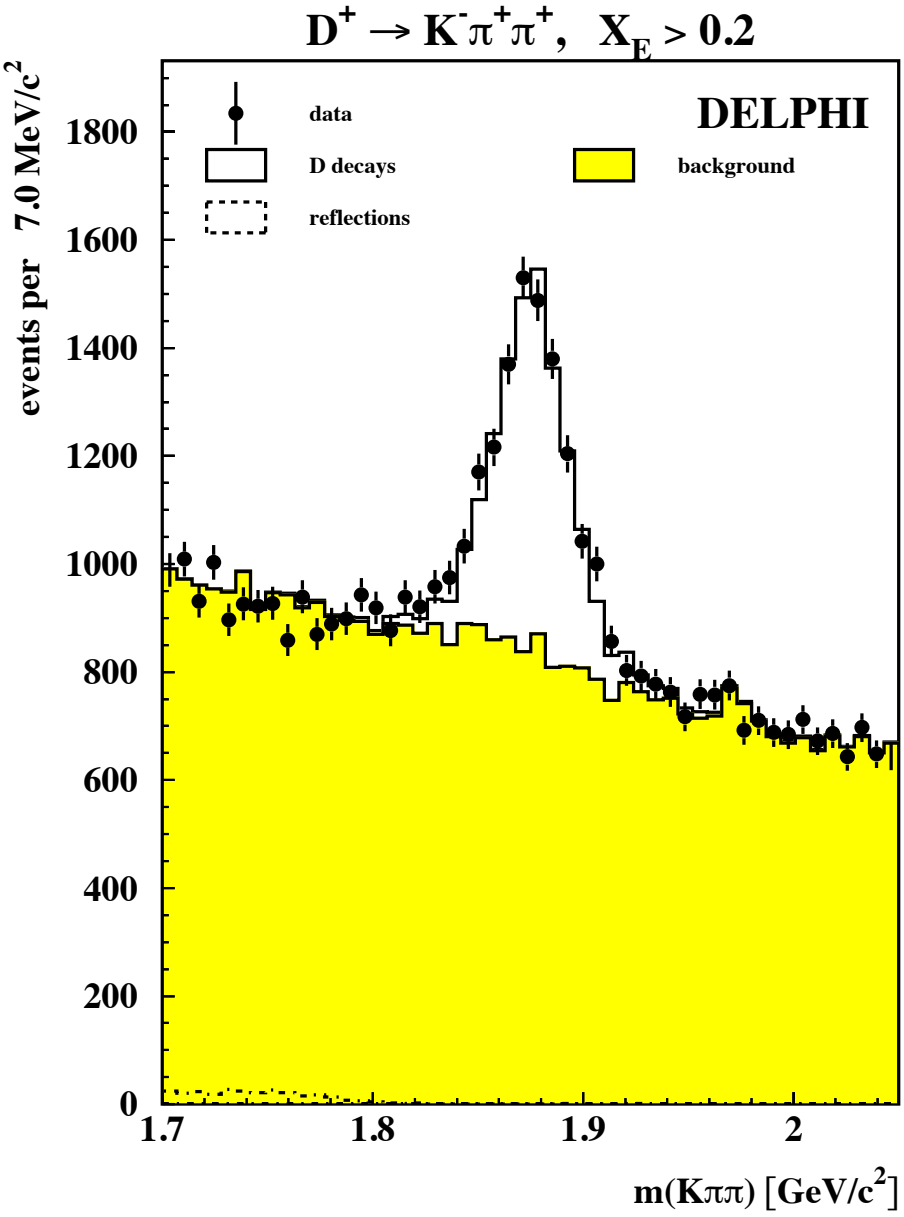

Figure 4: *Invariant $K\pi\pi$ mass spectra showing the D^+ mass signal.*

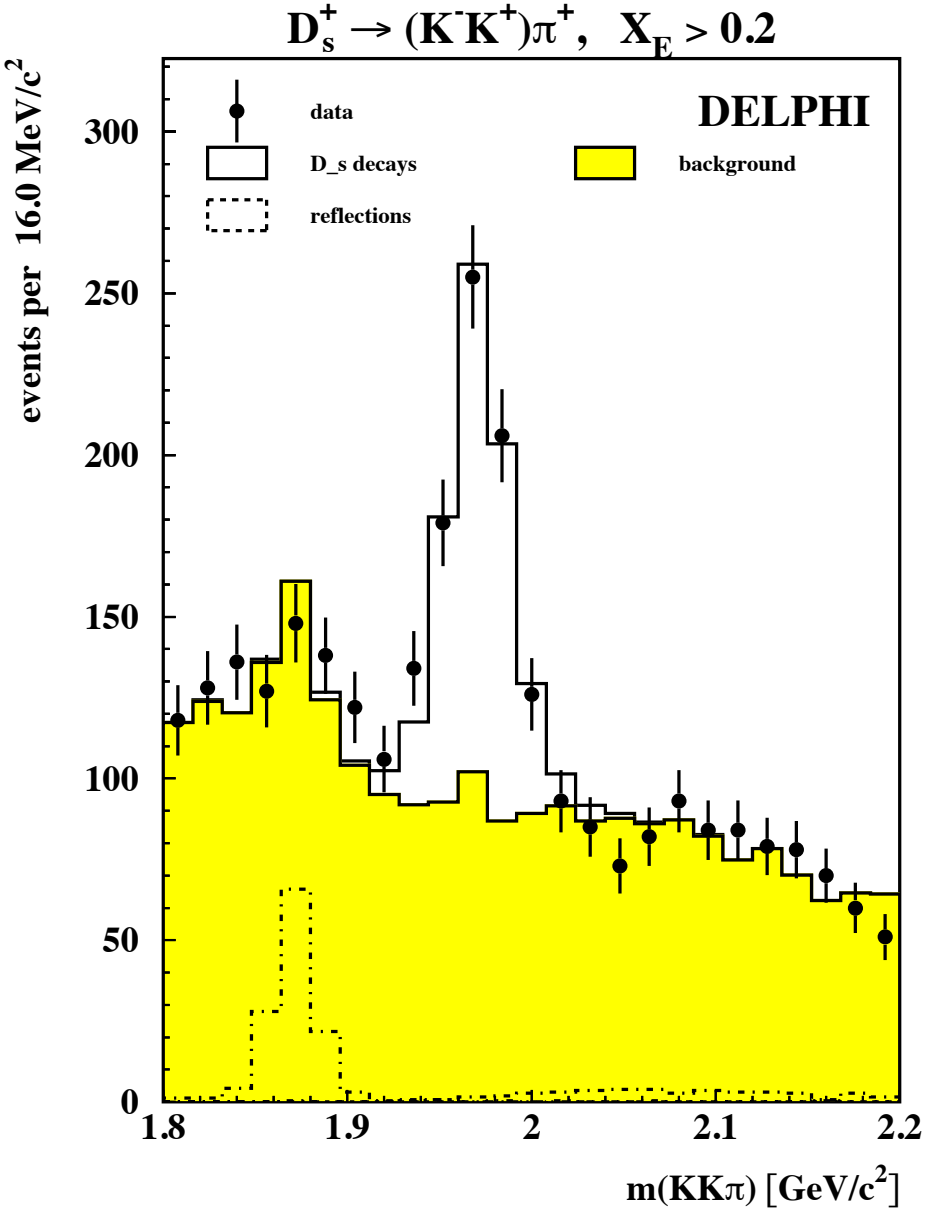

Figure 5: *Invariant mass spectra for the decay* $D_s^+ \to \phi(1020)\pi^+$. *The contributions from* D^{*+} *decays are described in the test.*

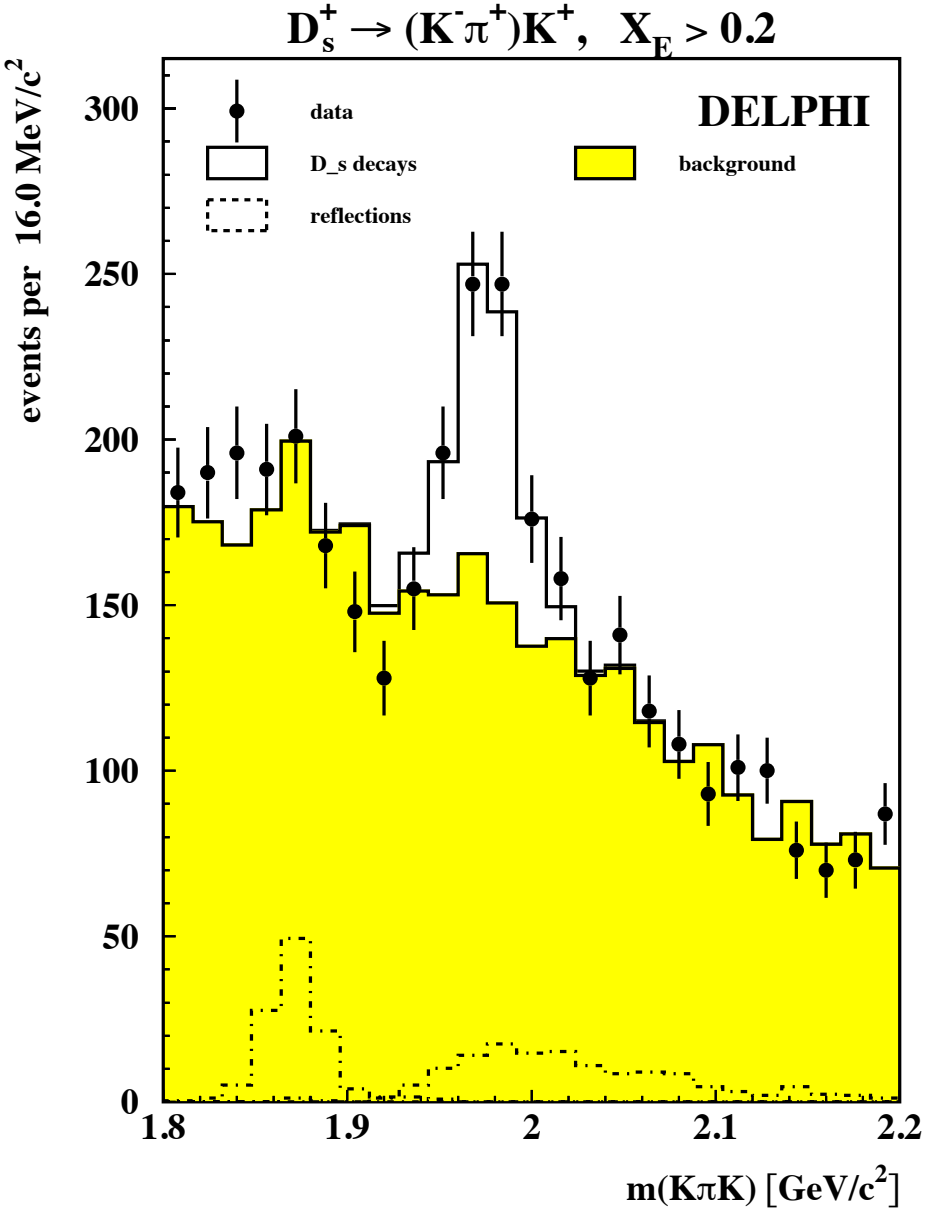

Figure 6: *Invariant mass spectra for the decay* $D_s^+ \to \bar{K}^*(892)K^+$. *The contributions from* D^{*+} *decays are described in the test.*

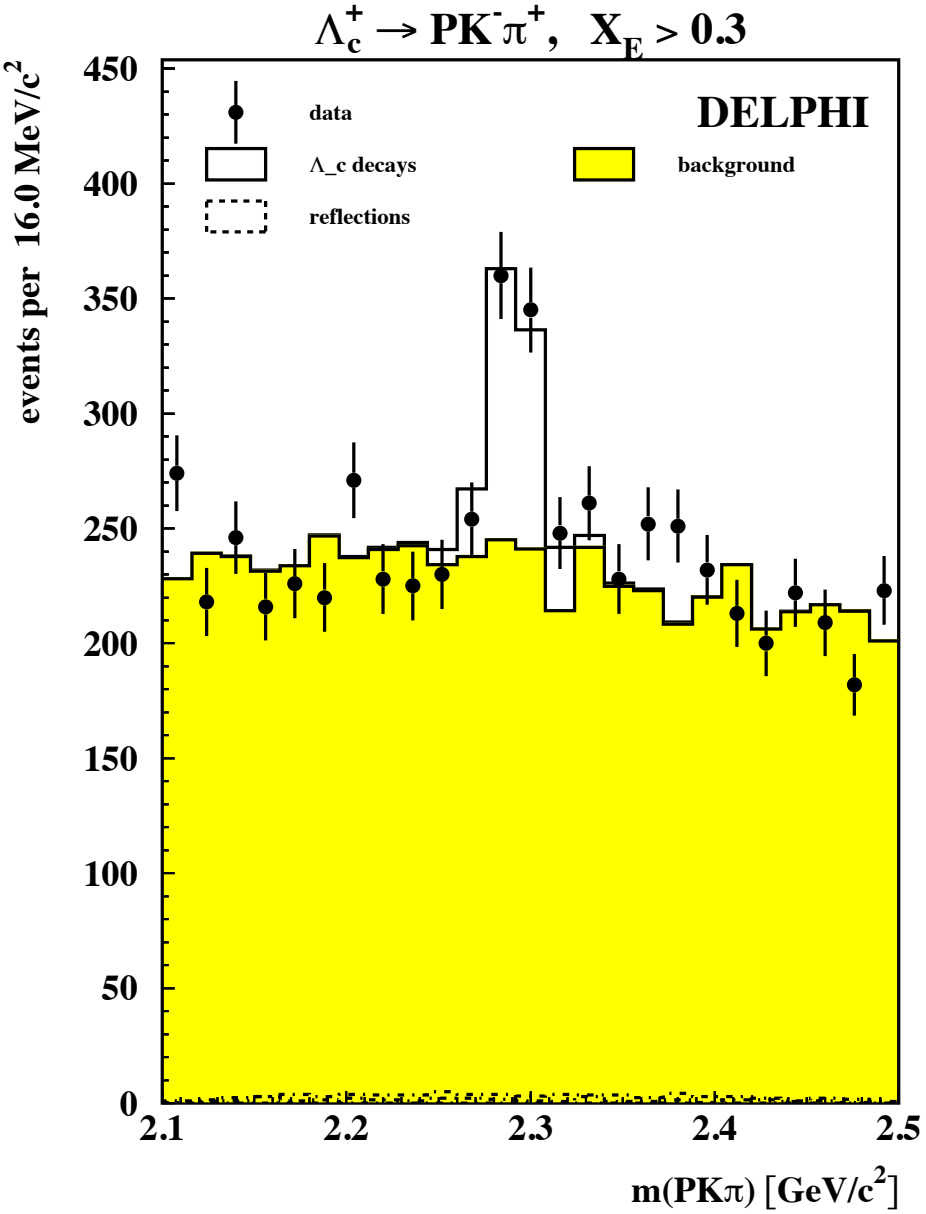

Figure 7: *Invariant mass spectra for the decay* $\Lambda_c^+ \to pK^-\pi^+$.

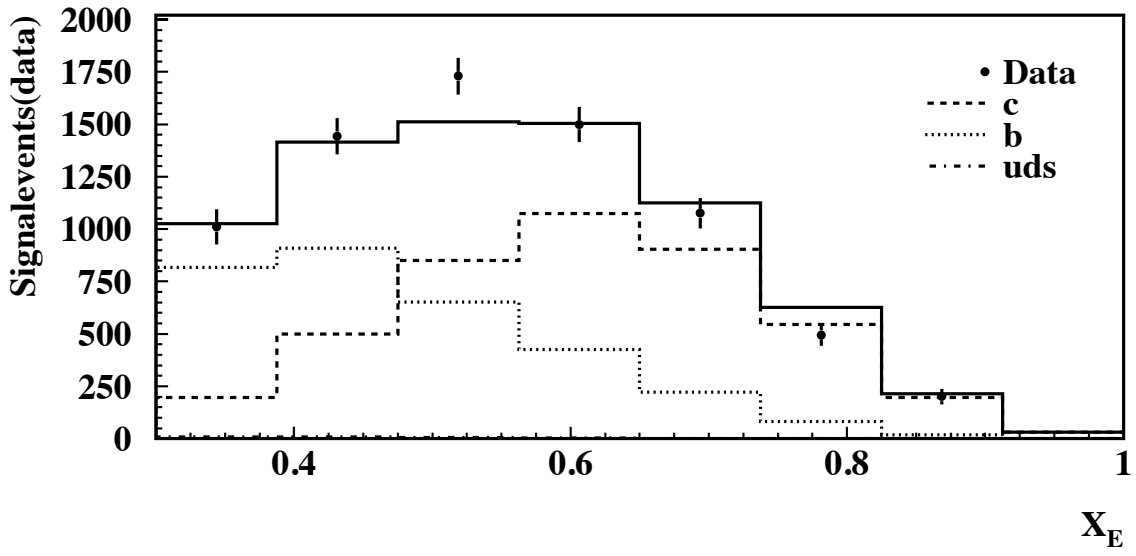

Figure 8: *Background subtracted X_E spectra for the decay $D^0 \to K^-\pi^+$. No efficiency correction is applied. The reconstructed Monte Carlo spectra for $b\bar{b}$ and $c\bar{c}$ events is scaled in order to reproduce the fit results as described in the text.*

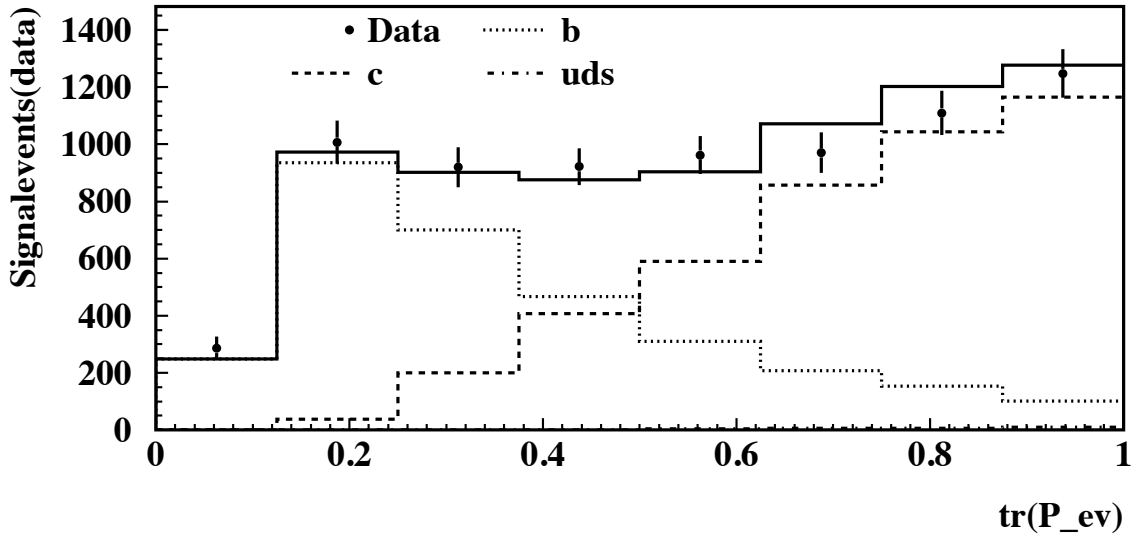

Figure 9: *Background subtracted $tr(\mathcal{P}_{ev})$ spectra for the decay $D^0 \to K^-\pi^+$. No efficiency correction is applied. The reconstructed Monte Carlo spectra for $b\bar{b}$ and $c\bar{c}$ events is scaled in order to reproduce the fit results as described in the text.*

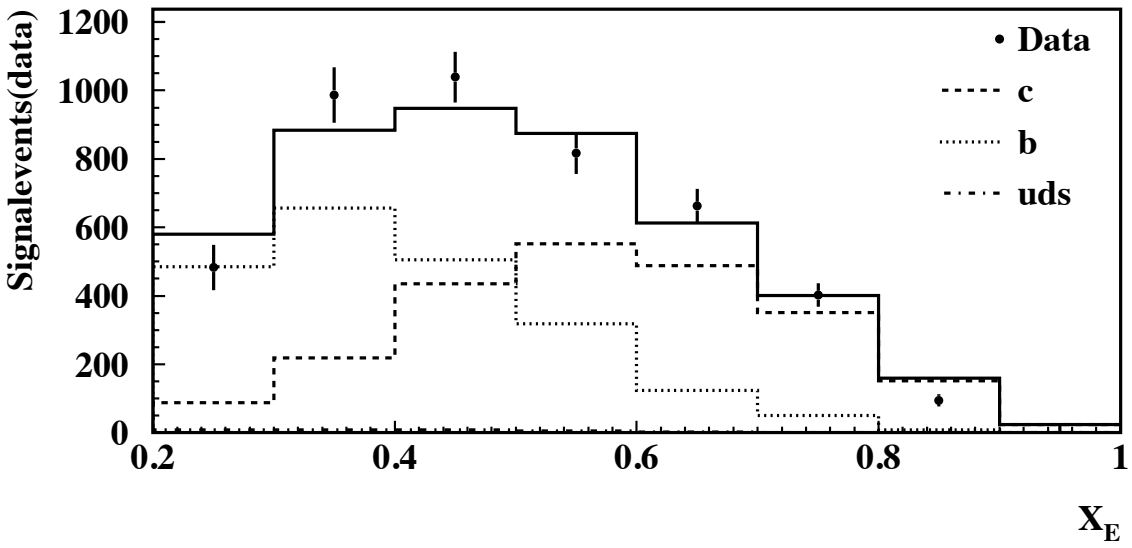

Figure 10: *Background subtracted X_E spectra for the decay $D^+ \to K^-\pi^+\pi^+$. No efficiency correction is applied. The reconstructed Monte Carlo spectra for $b\bar{b}$ and $c\bar{c}$ events is scaled in order to reproduce the fit results as described in the text.*

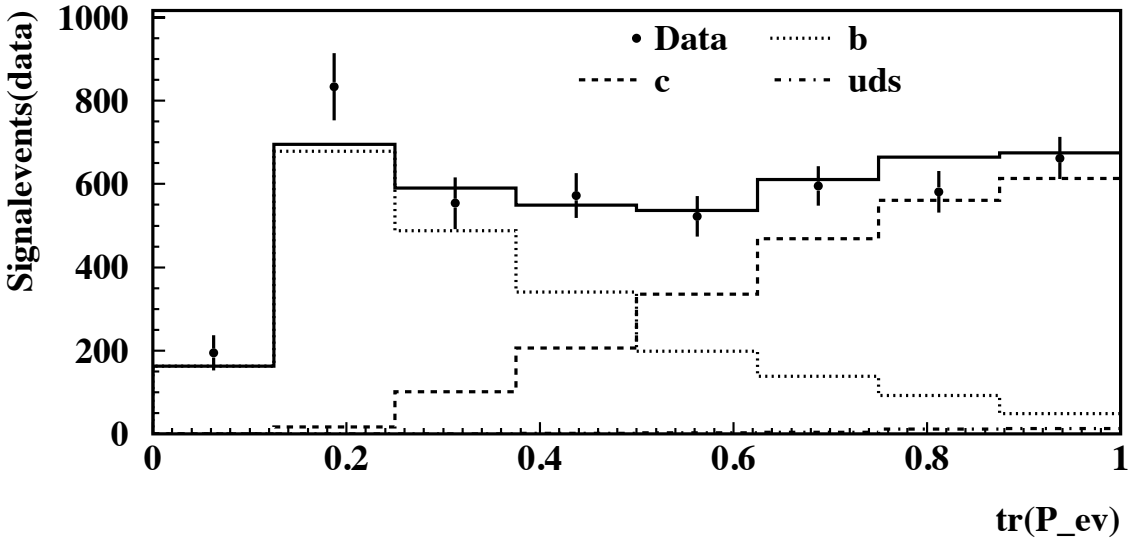

Figure 11: *Background subtracted $tr(\mathcal{P}_{ev})$ spectra for the decay $D^+ \to K^-\pi^+\pi^+$. No efficiency correction is applied. The reconstructed Monte Carlo spectra for $b\bar{b}$ and $c\bar{c}$ events is scaled in order to reproduce the fit results as described in the text.*

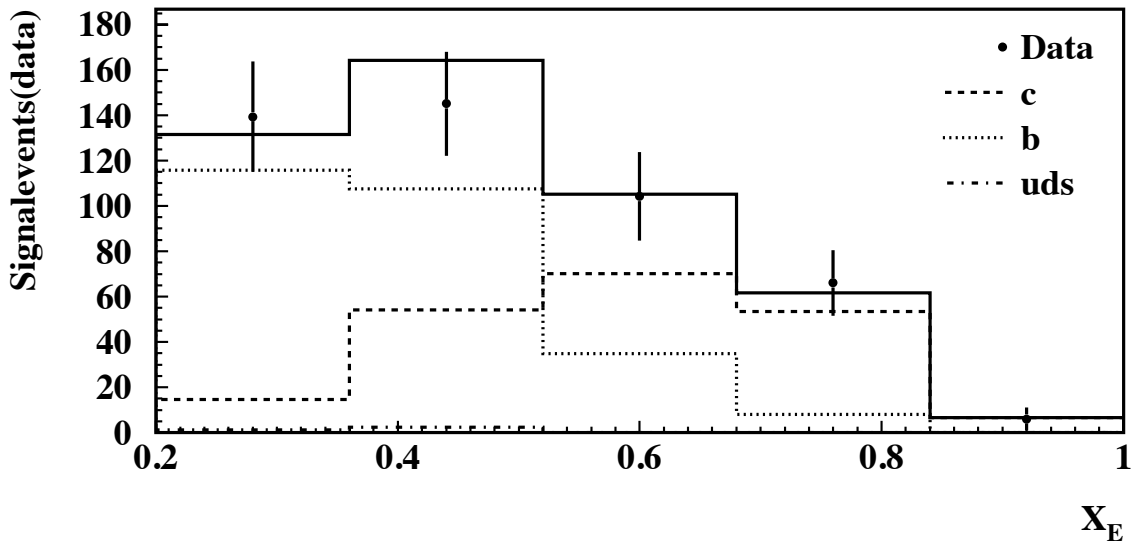

Figure 12: *Background subtracted X_E spectra for the decay $D_s^+ \to \phi(1020)\pi^+$. No efficiency correction is applied. The reconstructed Monte Carlo spectra for $b\bar{b}$ and $c\bar{c}$ events is scaled in order to reproduce the fit results as described in the text.*

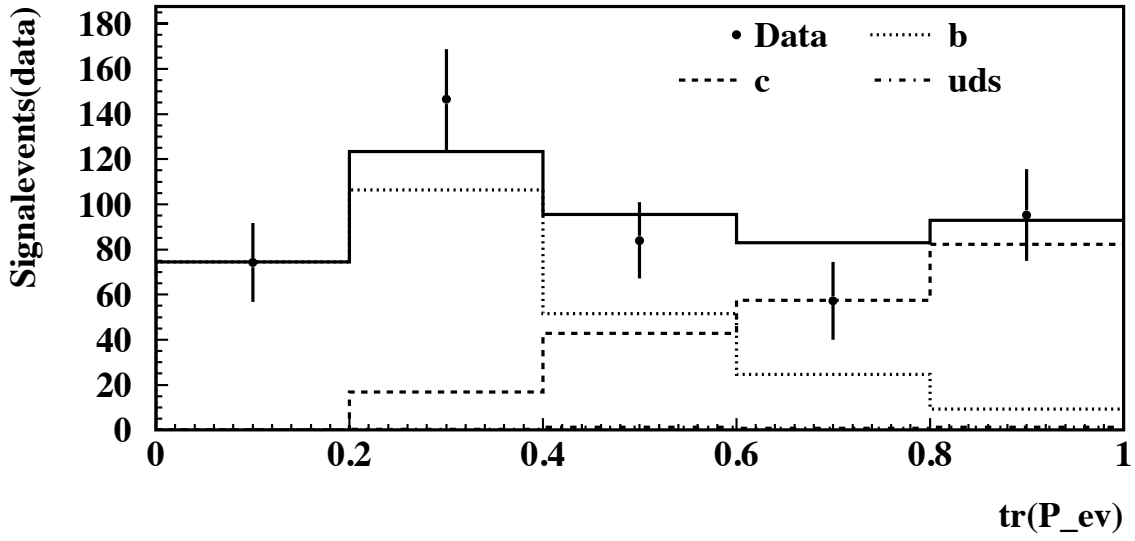

Figure 13: *Background subtracted $tr(\mathcal{P}_{ev})$ spectra for the decay $D_s^+ \to \phi(1020)\pi^+$. No efficiency correction is applied. The reconstructed Monte Carlo spectra for $b\bar{b}$ and $c\bar{c}$ events is scaled in order to reproduce the fit results as described in the text.*

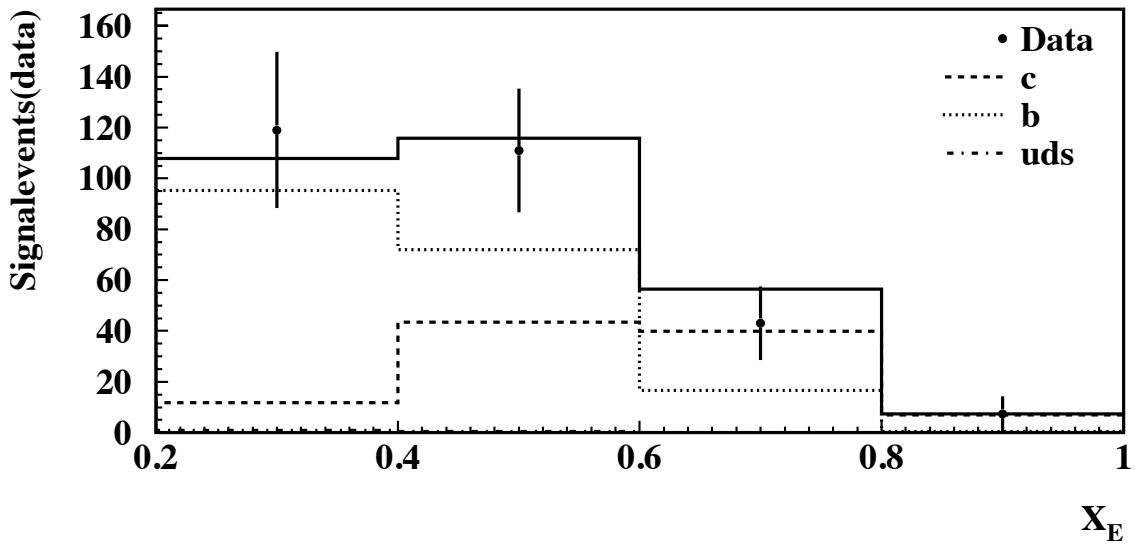

Figure 14: *Background subtracted X_E spectra for the decay $D_s^+ \to \bar{K}^*(892)K^+$. No efficiency correction is applied. The reconstructed Monte Carlo spectra for $b\bar{b}$ and $c\bar{c}$ events is scaled in order to reproduce the fit results as described in the text.*

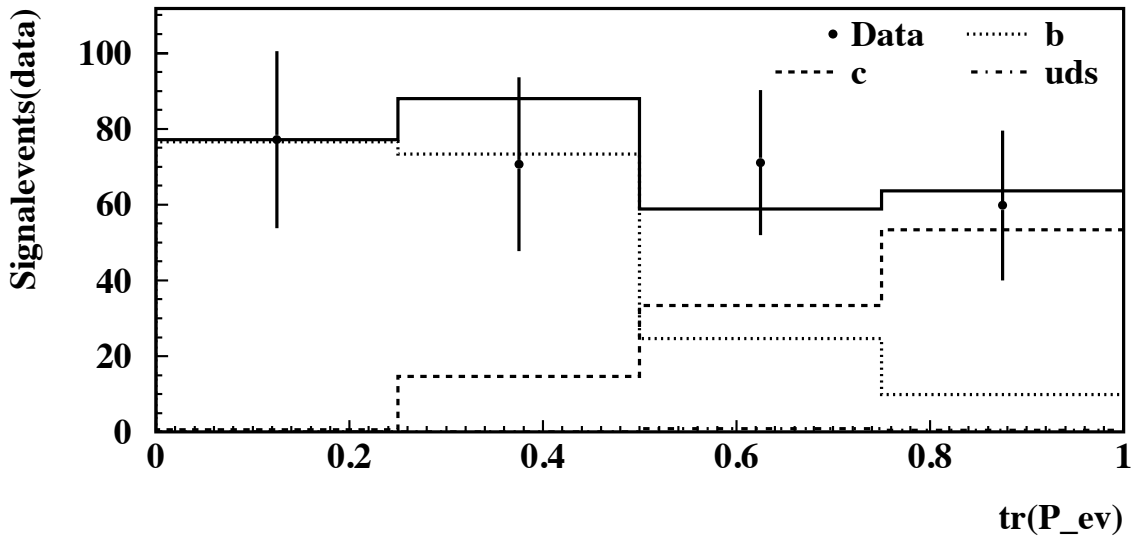

Figure 15: *Background subtracted $tr(\mathcal{P}_{ev})$ spectra for the decay $D_s^+ \to \bar{K}^*(892)K^+$. No efficiency correction is applied. The reconstructed Monte Carlo spectra for $b\bar{b}$ and $c\bar{c}$ events is scaled in order to reproduce the fit results as described in the text.*

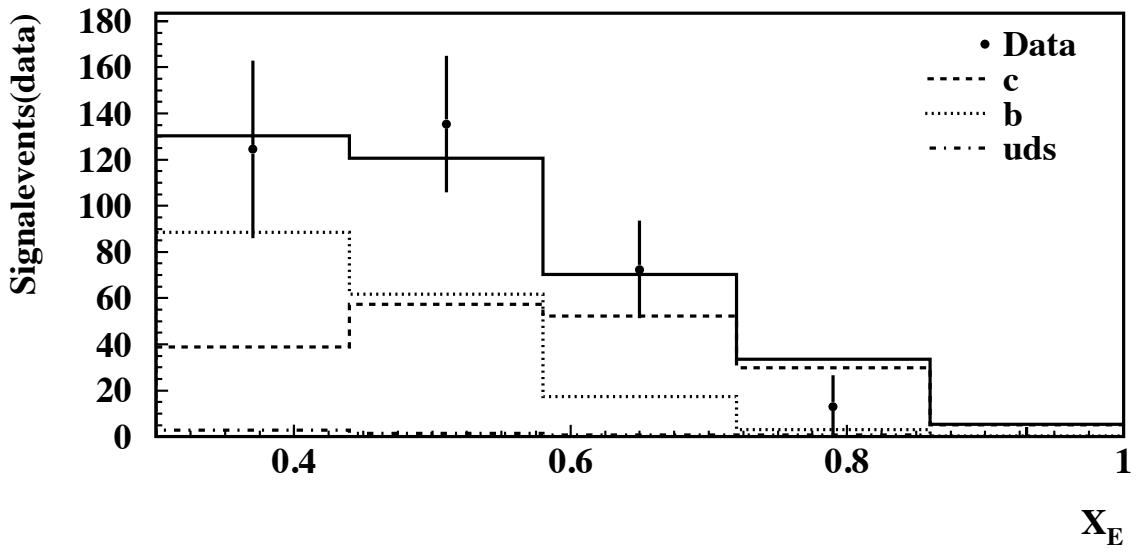

Figure 16: *Background subtracted X_E spectra for the decay $\Lambda_c^+ \to pK^-\pi^+$. No efficiency correction is applied. The reconstructed Monte Carlo spectra for $b\bar{b}$ and $c\bar{c}$ events is scaled in order to reproduce the fit results as described in the text.*

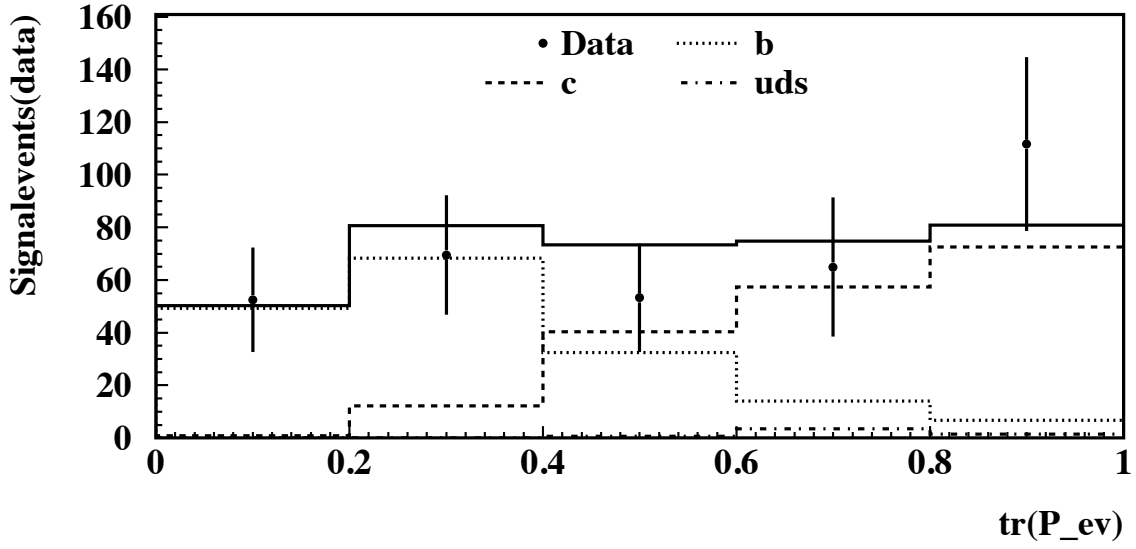

Figure 17: *Background subtracted $tr(\mathcal{P}_{ev})$ spectra for the decay $\Lambda_c^+ \to pK^-\pi^+$. No efficiency correction is applied. The reconstructed Monte Carlo spectra for $b\bar{b}$ and $c\bar{c}$ events is scaled in order to reproduce the fit results as described in the text.*

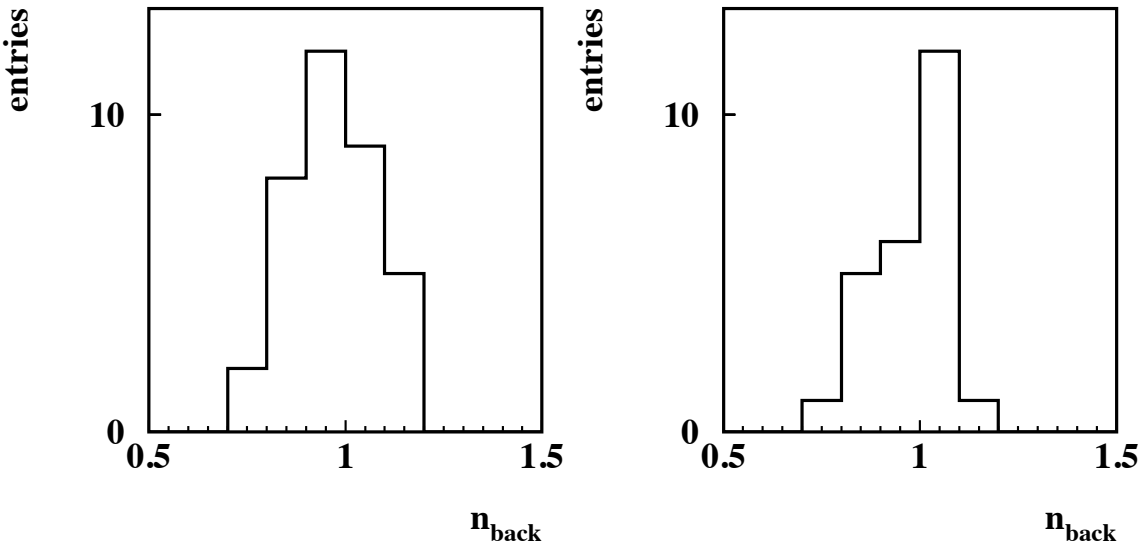

Figure 18: *Background normalisations for the D^+ (left) and the D^0 (right) resulting from the final fit.*

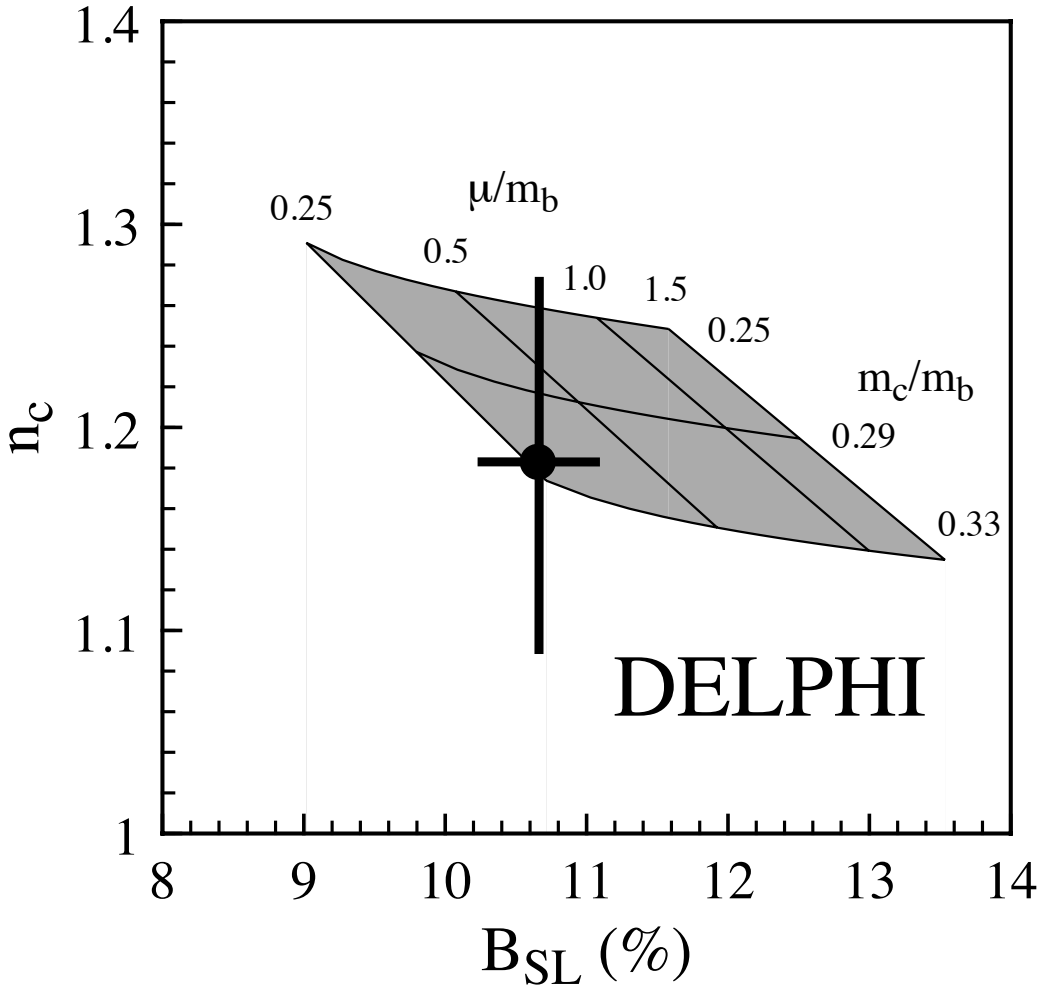

Figure 19: *A comparison of n_c and B_{SL} to the theoretical allowed region [23]. The area is representing the region predicted by theory in the on-shell renormalisation scheme for different values of m_c/m_b and of the renormalisation scale μ/m_b.*